Article

SOURCE DATA | TRANSPARENT PROCESS | OPEN ACCESS

EMBO reports

A dual-function SNF2 protein drives chromatid resolution and nascent transcripts removal in mitosis

Catarina Carmo[1,†], João Coelho[1,†], Rui D Silva[2], Alexandra Tavares[1], Ana Boavida[1,†], Paola Gaetani[1], Leonardo G Guilgur[1], Rui Gonçalo Martinho[2,3] & Raquel A Oliveira[1,4,*]

Abstract

Mitotic chromatin is largely assumed incompatible with transcription due to changes in the transcription machinery and chromosome architecture. However, the mechanisms of mitotic transcriptional inactivation and their interplay with chromosome assembly remain largely unknown. By monitoring ongoing transcription in *Drosophila* early embryos, we reveal that eviction of nascent mRNAs from mitotic chromatin occurs after substantial chromosome compaction and is not promoted by condensin I. Instead, we show that the timely removal of transcripts from mitotic chromatin is driven by the SNF2 helicase-like protein Lodestar (Lds), identified here as a modulator of sister chromatid cohesion defects. In addition to the eviction of nascent transcripts, we uncover that Lds cooperates with Topoisomerase 2 to ensure efficient sister chromatid resolution and mitotic fidelity. We conclude that the removal of nascent transcripts upon mitotic entry is not a passive consequence of cell cycle progression and/or chromosome compaction but occurs via dedicated mechanisms with functional parallelisms to sister chromatid resolution.

Keywords cohesin; condensin; mitotic transcription; SNF2 family; topoisomerase 2

Subject Categories Cell Cycle; Chromatin, Transcription & Genomics

DOI 10.15252/embr.202256463 | Received 18 November 2022 | Revised 28 June 2023 | Accepted 3 July 2023 | Published online 18 July 2023

EMBO Reports (2023) 24: e56463

Introduction

Mitotic chromosome assembly is essential for faithful genome distribution during mitosis. Defects in this process can damage dividing chromosomes, causing DNA breaks and genetic instability. This process encompasses changes in the compaction level and the topology of genome organisation, with concomitant global shutdown of most transcriptional activity (Gottesfeld & Forbes, 1997; Piskadlo & Oliveira, 2016). Nevertheless, how the structural changes that occur on mitotic chromatin impact its transcriptional state, while long postulated (Gottesfeld & Forbes, 1997), remains an open question.

The architectural reshaping of mitotic chromosomes is primarily mediated by the condensin complexes. Condensins are ring-like protein complexes known to extrude DNA molecules in an ATP-dependent manner (Ganji *et al*, 2018; Davidson *et al*, 2019; Kim *et al*, 2019), thereby leading to chromosome compaction. This process occurs with the concurrent resolution of sister chromatids, driven by two primary mechanisms: (i) the removal of protein-mediated linkages around DNA molecules, by the cohesin destabilising factor WAPL, which removes the molecular glue from chromosome arms (Losada *et al*, 1998; Sumara *et al*, 2000; Gimenez-Abian *et al*, 2004; Gandhi *et al*, 2006; Kueng *et al*, 2006); and (ii) the resolution of topological DNA–DNA links (e.g. catenations), by Topoisomerase 2 (Top2), which introduces a dsDNA break in one of the chromatids, allows for strand passage, and reseals the break (Pommier *et al*, 2016). Condensin-mediated chromosome compaction and removal of cohesin from chromosome arms aid in this process by positioning DNA molecules in a manner that biases Top2 activity towards the decatenation of DNA–DNA intertwines (Baxter *et al*, 2011; Sen *et al*, 2016; Piskadlo *et al*, 2017; Piskadlo & Oliveira, 2017).

Alongside these structural changes, mitotic chromosomes switch off most of their transcriptional activity (Gottesfeld & Forbes, 1997). In some cell types, such as the rapid divisions of early *Drosophila* embryos, entry into mitosis dictates abortion of ongoing transcription (Shermoen & O'Farrell, 1991; Rothe *et al*, 1992). The mechanisms that drive transcription termination/abortion and how they relate to the structural changes remain poorly understood. Recent studies propose that cohesin release contributes to the removal of active RNA Polymerase II (PolII) from chromosomes since abnormal cohesin retention is sufficient to accumulate active PolII along chromosome arms (Perea-Resa *et al*, 2020). Chromosome compaction is

1 Instituto Gulbenkian de Ciência, Oeiras, Portugal
2 Algarve Biomedical Center Research Institute (ABC-RI) and Faculty of Medicine and Biomedical Sciences (FMCB), Universidade do Algarve, Faro, Portugal
3 Department of Medical Sciences (DCM) and Institute for Biomedicine (iBiMED), Universidade de Aveiro, Aveiro, Portugal
4 Católica Biomedical Research Centre, Católica Medical School, Universidade Católica Portuguesa, Lisbon, Portugal
*Corresponding author. Tel: +351 21 4464690; E-mail: raaoliveira@ucp.pt
†These authors contributed equally to this work
‡Present address: Istituto di Biochimica e Biologia Cellulare, Consiglio Nazionale delle Ricerche, Naples, Italy

also assumed to actively or passively contribute to the switch off of transcription (Gottesfeld & Forbes, 1997), although this remains untested. The loop extrusion activity of SMC complexes (Ganji *et al*, 2018; Davidson *et al*, 2019; Kim *et al*, 2019; in particular of condensin) is a likely candidate to stall PolII or drive its eviction. Accordingly, condensin is often found at transcription termination sites in yeast mitotic chromosomes and is proposed to contribute to transcript release (Nakazawa *et al*, 2019). Moreover, mitotic bookmarking by TATA-binding protein (TBP) depends on local condensin inactivation (Xing *et al*, 2008). However, studies in bacteria showed that condensins can bypass the transcriptional machinery despite a reduction of speed upon their encounter (Brandao *et al*, 2019). Thus, it remains unclear if condensin loading on mitotic chromosomes influences the transcription cycle in metazoans.

In parallel to changes in chromosome organisation, regulation of the transcriptional machinery offers a direct layer of regulation of transcriptional switch-off. For example, *in vitro* studies support that biochemical inactivation of the basal transcription machinery, driven by Cdk1-mediated phosphorylation, prevents *de novo* transcription initiation (Segil *et al*, 1996; Bellier *et al*, 1997; Gebara *et al*, 1997; Akoulitchev & Reinberg, 1998; Long *et al*, 1998) but the prevalence of this inhibition *in vivo* remains unclear. Recent studies in human cells demonstrated that the transcription initiation inhibitor Gdown1 gains access to chromatin solely during mitosis to repress mitotic transcription (Ball *et al*, 2022). The human transcription termination factor 2 (TTF2) was also shown to be mostly cytoplasmic during interphase, gaining access to chromatin in mitosis to drive the removal of active PolII (Jiang *et al*, 2004). Additionally, phosphorylation of the RNA-to-DNA tethering protein SAF-A by the mitotic kinase Aurora B was shown to drive the eviction of transcripts from mitotic chromatin (Sharp *et al*, 2020). Recent studies have also proposed that specific mechanisms ensure promoter clearance upon mitotic entry, mediated by PolII activation of Top1, to release topological stress (Wiegard *et al*, 2021) or hyperactivation of P-TEFb, to enhance transcriptional elongation (Liang *et al*, 2015).

However, and despite these findings, it remains unclear how these pathways impact transcription dynamics relative to cell cycle progression and concomitant changes in chromosome architecture, as this process has never been monitored in real time. Using live-cell imaging of ongoing transcription in dividing *Drosophila* early embryos, we show that condensin-I-mediated compaction does not drive mitotic transcription inactivation (MTI). Instead, we reveal that the SNF2 helicase-like protein Lds, the *Drosophila* orthologue of human TTF2 (Liu *et al*, 1998), ensures prompt eviction of nascent RNAs from mitotic chromatin. In parallel to MTI, Lds also aids DNA decatenation of sister chromatid intertwines. We conclude Lds holds a dual function in mitotic chromosomes, uncovering unforeseen functional parallelisms between mitotic transcription inactivation and sister chromatid resolution.

Results

A genetic screen for modifiers of cohesion loss uncovers *lodestar* as a strong suppressor of cohesion defects

We have previously established a genetic screen to find modulators of sister chromatid cohesion (Silva *et al*, 2018). This screen uses the morphology defects in *Drosophila* wings obtained upon depletion of the cohesin stabiliser separation anxiety (san) (Williams *et al*, 2003; Hou *et al*, 2007; Ribeiro *et al*, 2016; Rong *et al*, 2016). Changes in the wing morphology phenotypes are then used to unbiasedly identify conditions that could either enhance or suppress the defects associated with cohesion loss (Silva *et al*, 2018). In a subsequent search for additional cohesion modifiers, using the same approach, we uncovered the SNF-2 helicase-like lodestar (lds), the putative orthologue of the human TTF2 (Liu *et al*, 1998), as a modulator of the defects associated with cohesion loss. When san RNAi was driven by a driver specific to the wing imaginal disc pouch/blade region (Nubbin Gal4, nub-Gal4) (Fig 1A), flies ecloded with significant adult wing abnormalities (Fig 1B and C; Ribeiro *et al*, 2016; Silva *et al*, 2018). However, co-expression of san RNAi with lds RNAi (but not with mCherry RNAi) efficiently suppressed these abnormalities and wings were significantly closer to normal morphology (Fig 1B and C). Hence, depletion of Lds is likely a potent suppressor of cohesion defects observed after san RNAi.

Lds has been previously described as a maternal-effect gene whose loss-of-function mutations are associated with mitotic defects during early embryogenesis (Girdham & Glover, 1991). Additionally, a dominant gain of function allele was found to impair meiotic chromosome segregation (Szalontai *et al*, 2009). However, it remains unknown how this protein contributes to the fidelity of nuclear division.

Lds is associated with mitotic chromatin and required for mitotic fidelity across various tissues

We next sought out to investigate whether Lds is also required for the fidelity of mitosis in somatic tissues. We used live-cell imaging

Figure 1. Depletion of Lds strongly suppresses the defects associated with cohesin loss.

A Tissue-specific RNAi in the pouch of the larvae wing imaginal discs using the nubbin-Gal4 driver and the upstream activating sequence (UAS)/Gal4 system. Black arrows point to both the larvae and adult notum and to the wing pouch responsible for the development of the adult wing blade.

B Representative images of *Drosophila* adult wings that resulted from larvae wing imaginal discs expressing a control RNAi (mCherry RNAi), a *lds* RNAi, or co-expressing *san* RNAi with control RNAi (san RNAi control RNAi) or with *lds* RNAi (san RNAi lds RNAi).

C Quantification of *Drosophila* adult wing phenotypes expressing individual control RNAi or *lds* RNAi transgenes, co-expressing *san* RNAi and control RNAi, or co-expressing *san* RNAi and *lds* RNAi. Classes used for phenotypic quantification were previously described in (Silva *et al*, 2018), and a representative example for each class is shown on top of the graph: class 1 (wild-type wings); class 2 (adult wings with weak developmental defects); class 3 (adult wings with moderate developmental defects; *san* RNAi-like wing phenotype); class 4 (highly abnormal adult wings); and class 5 (absence or vestigial adult wings). Representative images shown in (B) of adult wings co-expressing *san* RNAi and control RNAi correspond to class 3, whereas wings co-expressing *san* RNAi and *lds* RNAi correspond to class 2. The results represent the mean of three independent biological experiments, with each experiment denoted by a black dot; statistical analysis was performed using one-way ANOVA with Bonferroni's multiple comparison test; *n* represents the total number of scored flies per condition.

Source data are available online for this figure.

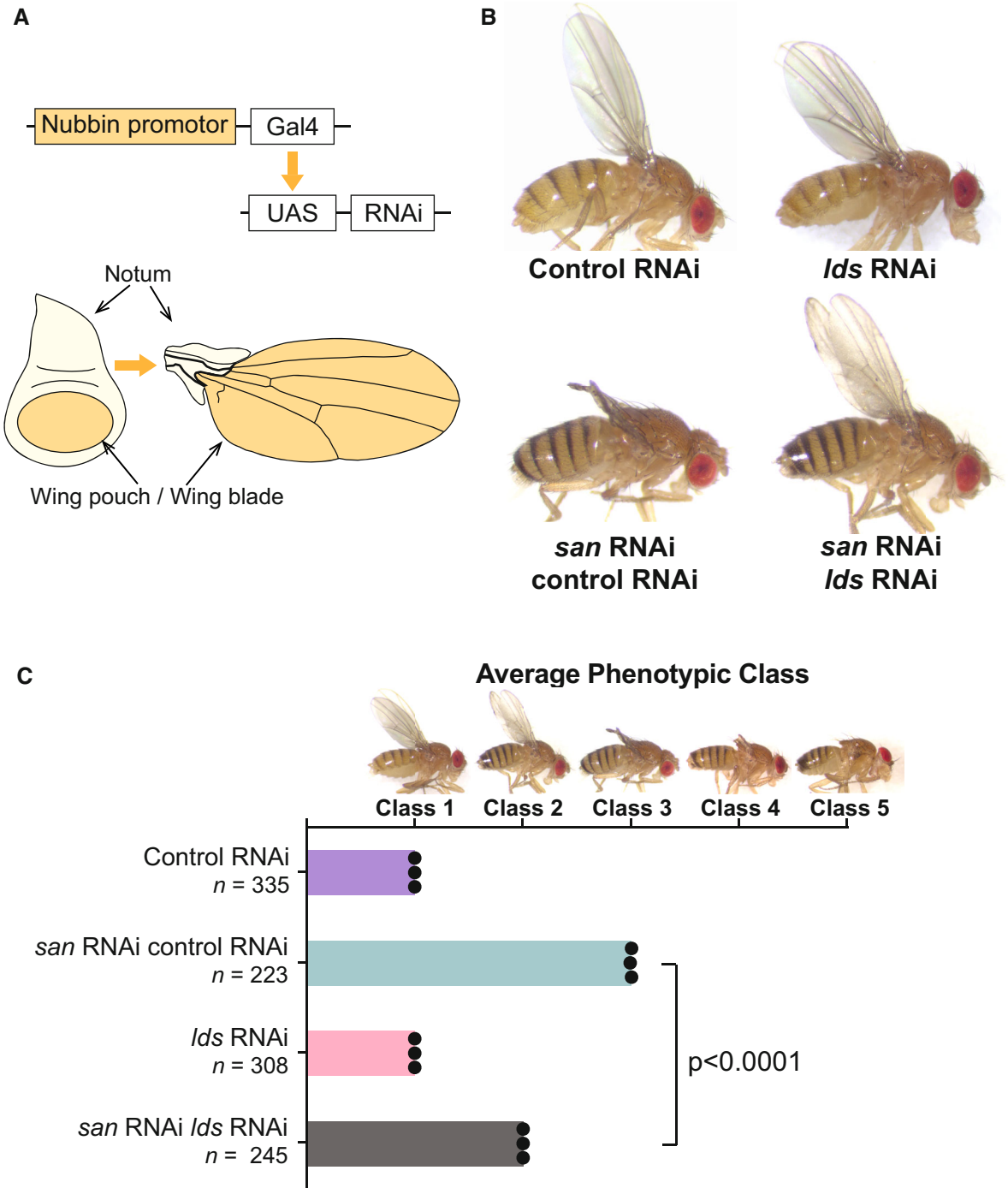

Figure 1.

analysis to probe for the accuracy of mitosis upon RNAi-mediated depletion of Lds in the developing wing disc. Nub-Gal4 was used to drive RNAi for lds (alone), specifically in the wing pouch, leading to local depletion of Lds (Fig EV1A). We found that in the absence of Lds, the nuclear division is slightly delayed and severely compromised, with a high frequency of anaphase bridges at mitotic exit (Fig 2A–C). Defective mitosis was also observed in the embryos upon depletion of maternal Lds. Using the nanos Gal4 (nos-Gal4) to induce lds RNAi in the germline and early embryos (Fig EV1B), we observed a significant reduction of egg hatching (Fig EV1C). This is accompanied by severe defects of the early mitotic divisions (Fig EV1D and E), which can be partially rescued by ectopic addition of Lds (Fig EV1F–H). Our results confirm that Lds is required for mitotic fidelity in various tissues, similar to what was previously reported (Girdham & Glover, 1991).

To gain further insight into the mitotic functions of Lds, we generated flies carrying a C-terminal EGFP-fusion at the endogenous lds locus (using CRISPR-Cas9-based genome editing). The resulting

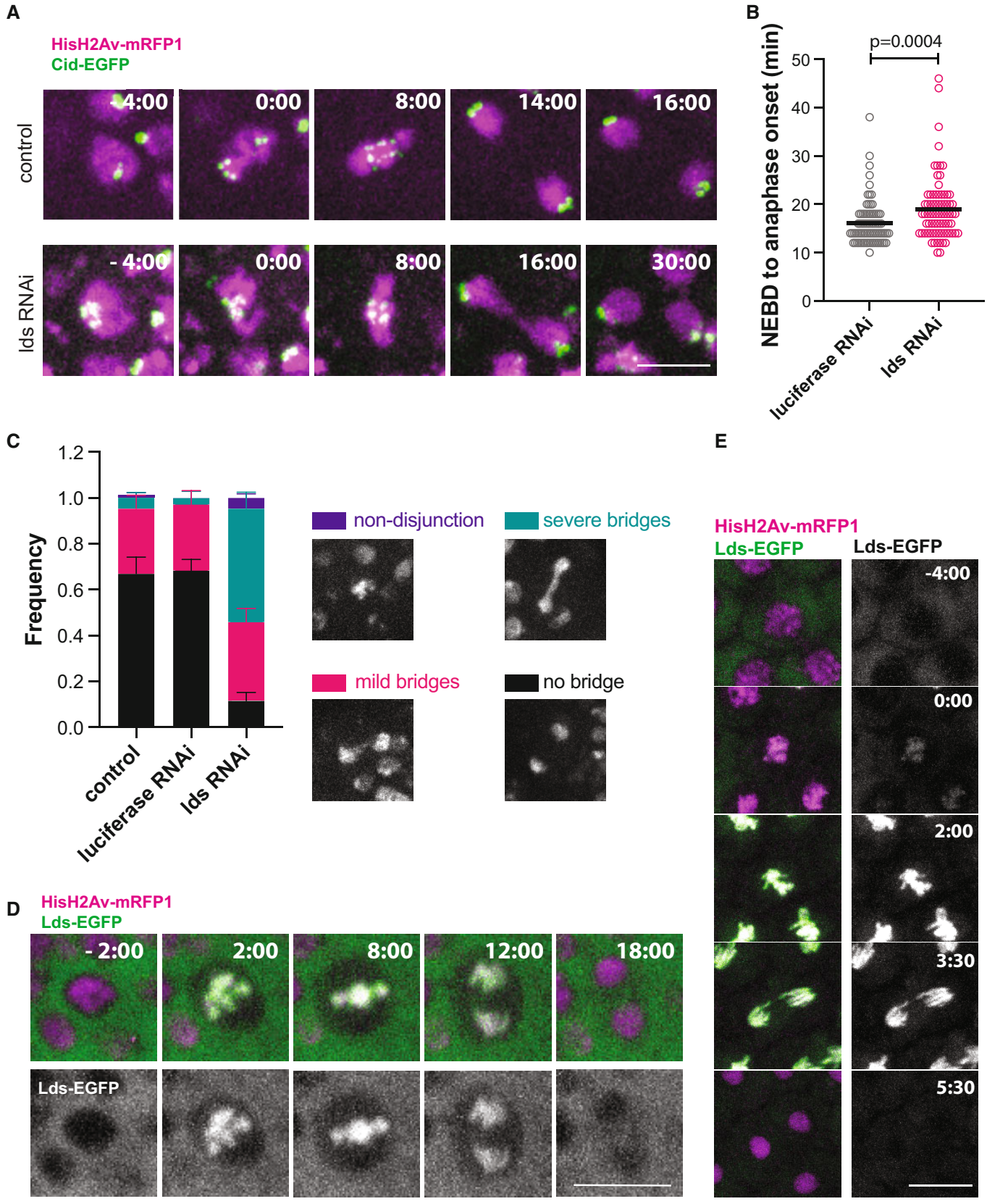

Figure 2.

Figure 2. Lds is associated with mitotic chromatin and required for mitotic fidelity.

A Representative images of cells in the wing disc pouch upon nub-Gal4-mediated RNAi for lds (bottom) compared with a nub-Gal4 control (top). Cells also express HisH2AvD-mRFP1 (magenta) and centromeric marker cid-EGFP (green); times (min:sec) are relative to NEBD; scale bar is 5 μm and applies to all images.

B Mitotic timing defined from NEBD to anaphase onset; each dot represents a different cell ($n = 77$ cells from at least six independent movies per condition); black lines represent mean; statistical analysis was performed using the nonparametric Mann–Whitney test.

C Frequency of segregation defects during mitosis in *Drosophila* wing discs. Graph depicts the average frequency of segregation defects observed, represented as mean ± s.e.m. ($n = 6$ discs wild-type control; $n = 5$ discs luciferase RNAi; $n = 8$ discs lds RNAi; average of 16 cells measured per disc); Examples of segregation defects are shown in the left and presence of DNA bridges was scored as follows: no bridge, when no bridges could be identified; mild bridge; when a fine bridge is observed but resolved within 2–4 min after AO; severe bridge; when thick DNA bridges are observed that remain unresolved for > 4 min after AO; nondisjunction for cases where chromosomes remain arrested in metaphase or exit mitosis to form a single nucleus.

D, E Localisation of Lds-EGFP (green) throughout mitosis in *Drosophila* wing discs (D) and *Drosophila* syncytial embryos (E). Times are relative to NEBD, flies also express HisH2AvDmRFP1 (magenta).

Data information: Scale bars are 10 μm and apply to all images.
Source data are available online for this figure.

strain retains maximal female fertility, which reinforces the functionality of the tagged protein (Fig EV1C). When assessing Lds localisation in *Drosophila* dividing tissues, we observed that Lds is excluded from chromatin during interphase but gains access to mitotic chromatin around the time of nuclear envelope breakdown (NEBD), in both wing discs and syncytial embryos (Fig 2D and E). The chromatin levels of Lds are maximised during metaphase and decay as cells exit mitosis. These results suggest that Lds acts specifically on mitotic chromatin to ensure faithful genome partition. We, therefore, sought to investigate how Lds contributes to mitotic fidelity.

Lds mediates the timely release of RNA transcripts from mitotic chromatin

In vitro studies have previously demonstrated that Lds (also known as factor 2) has transcription termination activity (Price *et al*, 1987; Xie & Price, 1996, 1997, 1998). However, this activity has never been demonstrated *in vivo*, and it remains to be determined how it relates to a putative role in chromosome segregation. We focussed our analysis on establishing whether transcriptional changes upon mitotic entry could be defective in the absence of Lds. For this, we used *Drosophila* early embryos as a prime model system. Despite the reduced level of transcription (solely restricted to a minor wave of zygotic transcription; Tadros & Lipshitz, 2009), several tools allow for efficient monitoring of transcriptional dynamics by live-cell imaging. We used a system that enables the visualisation of a reporter transcript that carries MS2 loops at its 5′ and is expressed under the early zygotic gene *hunchback* (*hb*) promoter (Garcia *et al*, 2013). Upon transcription initiation in flies carrying MCP-EGFP, MCP binds the MS2 loops, and the GFP signal is readily detected at the transcription site, enabling the analysis of transcription in real time (Garcia *et al*, 2013). Using this approach, we monitored the time and kinetics of transcript release relative to mitotic progression and chromosome compaction. We found that in wild-type embryos, complete removal of the labelled nascent transcripts from chromatin was only observed following NEBD, considerably after the initiation of chromosome condensation (Figs 3A and B, and EV2). It is important to note that in most cases (~ 60%), mRNA signals are clearly observed in the cytoplasm, displaced from chromatin (Fig 3C). Considering that single mRNA molecules are not distinguishable from the cytoplasmic background, these findings indicate that multiple nascent mRNAs are detached from chromatin in bulk. Collectively, these findings suggest that transcript release may be mediated by active mechanisms that operate shortly after NEBD.

Then, we asked whether Lds could drive transcript release in these divisions. We monitored the kinetics of nascent mRNAs disappearance from chromatin in embryos depleted of Lds. When looking at the dynamics of ongoing transcription in these embryos, we observed that nascent mRNAs remain attached to mitotic chromatin for much longer in the absence of Lds, and full transcript release could only be detected on average ~ 3.5 min after NEBD (Fig 3A and B). This delay is partially restored upon ectopic addition of mRNA coding for an RNAi-resistant form of lds (Fig EV3A and B). Analysis of the kinetics of transcript removal reveals that in both controls and lds-depleted embryos, the number of transcripts

Figure 3. Lds, but not condensin I, is required for timely release of nascent transcripts in mitosis.

A Analysis of ongoing transcription monitored by MCP-EGFP labelled nascent transcripts on a reporter containing MS2 loops (green), in the referred experimental conditions. Flies also express H2AvD-mRFP1 (magenta). Scale bar is 10 μm and applies to all images.

B Time of clearance of MCP-labelled transcripts from mitotic chromatin, relative to NEBD. Each dot represents a single cell and black bars the mean; $n = 140$ (luciferase RNAi), 122 (lds RNAi), 150 (Cap-D2 RNAi) and 63 (barren^{TEV} after injection of TEV protease) nuclei, derived from 5 to 12 individual embryos per experimental condition. Statistical analysis was performed using the nonparametric Kruskal–Wallis test and Dunn's test for multiple comparisons.

C Frequency of the mode of disappearance of mRNA signal from mitotic chromatin in luciferase and lds RNAi embryos. Individual nuclei were followed and scored according to the mode that the GFP-labelled mRNA is removed from chromatin: bulk removal (when mRNA labelled transcripts could be detected in the cytoplasm; arrow in left panel); dimmed (when signal is progressively lost); on chromatin (when the signal is still present on the last metaphase figure). Graph depicts mean ± s.e.m. from 17 (luciferase RNAi) or 23 (lds RNAi) independent embryos; an average of 18 nuclei were scored per embryo. Legend depicts examples of each category, showing three consecutive images acquired at 30-s intervals.

D Frequency of anaphase figures with MCP-EGFP signals (labelling nascent transcripts) observed on/off mitotic chromatin. Graph depicts average from 15 (luciferase) and 17 (lds) independent movies. Error bars are s.e.m.

Source data are available online for this figure.

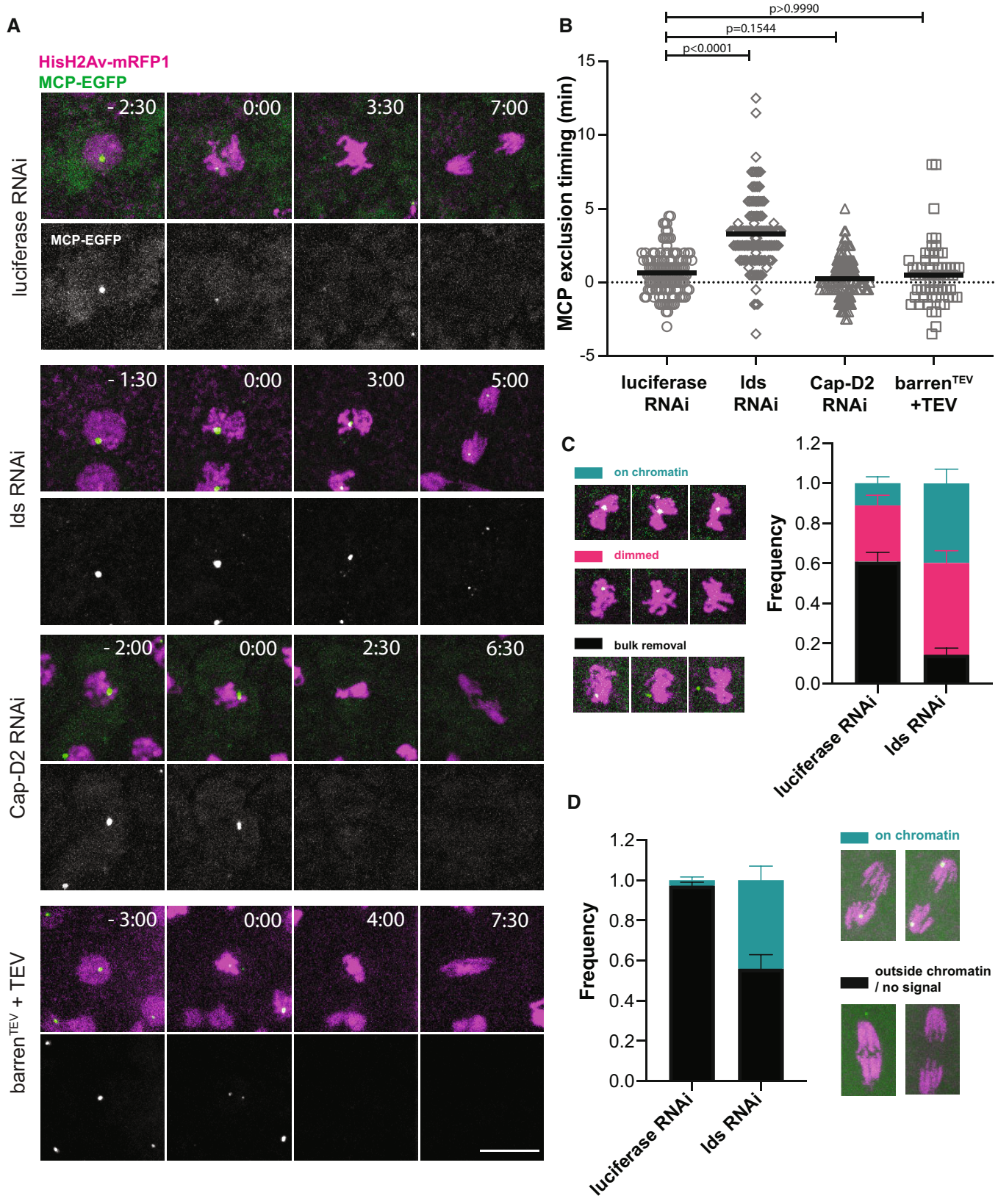

Figure 3.

detected on chromatin, monitored by the fluorescence of MCP-EGFP signal, starts to decrease shortly before NEBD (Fig EV3C). However, upon lds depletion, the rate of transcript removal occurs at a slower rate (Fig EV3C). Notably, the frequency of mRNAs removed in bulk is significantly decreased in lds RNAi embryos (14%), compared with controls (61%) (Fig 3C).

Consequently, while anaphases from control embryos rarely retain nascent mRNAs bound to chromatin, upon lds RNAi, we detected nascent mRNAs still attached in ~44% of anaphases, sometimes remaining throughout the entire cell division cycle (Fig 3D). This localisation is, in most cases, symmetrically placed and consistent with the reporter's location (i.e. ~1/3 of the left arm of chromosome 2 for the hb-MS2-lacz reporter, Fig EV3D). These observations imply that the detected mRNAs are still present at the active transcript site in the later stages of mitosis. Although we cannot formally exclude that transcript retention results from other perturbations on the transcription cycle (e.g. delay in the inhibition of transcription initiation), our results are more consistent with Lds driving active removal of nascent transcripts during mitosis. To confirm that Lds activity occurs globally on mitotic chromatin, we used different reporters with expression driven by the promoters of other early zygotic genes (*snail* and *even-skipped*). In both cases, we also detected a significant delay in transcript release in Lds-depleted embryos (Fig EV3E and F). Moreover, labelling of recently transcribed RNAs by EUTP incorporation reveals a significant enrichment on chromatin upon lds depletion (Fig EV3G and H). These findings support that removal of a wide range of engaged transcripts occurs via dedicated machinery, and not simply as a by-product of the structural changes that occur on the mitotic chromatin.

To confirm this notion, we then asked whether condensin I complex loading, enhanced around the time of NEBD (Oliveira *et al*, 2007), also contributes to transcript release. We tested this idea by analysing the time of removal of MCP-labelled transcripts from chromatin in embryos depleted for one of the condensin I subunits, Cap-D2. The prediction is that if condensin I activity drives transcript eviction, its depletion should alone induce a delay in nascent RNA removal. In contrast to this expectation, we observed that RNAi for Cap-D2 did not impose any noticeable delay in nascent mRNA eviction relative to controls (Fig 3A and B). Similar results were obtained upon acute inactivation of the kleisin subunit prior to mitotic entry (TEV-mediated cleavage of the condensin I subunit Barren (Piskadlo *et al*, 2017)). Using this approach, and although the frequency of severe anaphase bridges and mitotic defects was very high (Piskadlo *et al*, 2017), these changes in chromosome organisation were not associated with any delay in the timing of transcript release (Fig 3A and B). Altogether, these results suggest that loop extrusion mediated by condensin I complexes does not contribute to the eviction of RNAs from chromatin during mitosis and support the hypothesis that timely removal of nascent transcripts during mitosis relies on specific mechanisms, driven by the helicase-like protein Lds.

Failing to evict nascent transcripts is not the sole cause of the mitotic defects associated with the loss of Lds

Considering the high frequency of mitotic defects observed in embryos depleted of Lds, we asked whether abnormally trapped transcripts could be the source for the observed errors. We reasoned that if the segregation defects associated with the loss of Lds derive from transcriptionally dependent events, transcription inhibition should be sufficient to restore mitotic fidelity. To test this notion, we performed transcription inactivation experiments. We microinjected embryos with 1 mg/ml alpha-amanitin in early interphase (Fig 4A), which is sufficient to impair transcription, as evidenced by the absence of MS2-labelled reporter RNAs in the subsequent interphase (Fig EV4A–D). Transcription inhibition in wild-type embryos did not compromise mitotic fidelity (Fig 4B). This finding implies that, in contrast to prior reports (Staudt *et al*, 2006; Liang *et al*, 2008), ongoing transcription is not required for mitotic fidelity, at least within the short time frames of this experimental set-up.

Next, we used the same approach to inhibit transcription in lds RNAi embryos. This analysis revealed that in the presence of transcription (control H_2O injection), lds RNAi embryos present ~43% of abnormal anaphase figures (Fig 4B). Upon alpha-amanitin injection, the frequency of these defects is not significantly reduced (41%) (Fig 4B). These findings imply that the presence of trapped nascent mRNAs on mitotic chromatin is not the primary source of defects that compromise mitotic fidelity in Lds-depleted embryos.

Lds promotes sister chromatid resolution

Since transcription inhibition does not rescue the segregation defects observed upon depletion of Lds, we reasoned that those mitotic defects were likely to result from transcription-independent events. We thus hypothesised that Lds might hold additional roles in mitotic fidelity beyond the removal of nascent transcripts. We focussed on the fact that the most prominent phenotype was a high frequency of chromatin bridges to investigate whether Lds contributes to the resolution of sister chromatids.

To test this, we probed for potential genetic interactions of lds with other conditions known to be involved in the resolution of sister chromatids throughout mitosis. We envisioned two possible ways Lds contributes to the resolution of sister chromatids. One way could be via the stabilisation of cohesin-mediated linkages at the metaphase-anaphase transition, thereby hindering the efficient release of this proteinaceous glue. The second would imply a contribution to the removal of DNA–DNA ties (catenations), catalysed by topoisomerase 2 with the help of condensin I (Piskadlo & Oliveira, 2017). Following this rationale, we employed the same strategy presented above and used the modulation of wing morphology defects as a read-out for potential genetic interactions. Despite the high percentage of mitotic defects, depletion of Lds alone does not cause detectable adult wing morphology abnormalities, possibly due to compensatory proliferation pathways that ensure tissue homeostasis (Ryoo *et al*, 2004). We next probed for the effect of co-depletion of Lds with other players known to contribute to sister chromatid resolution. We found that removal of Lds could enhance the phenotype associated with overexpression of a modified version of cohesin where the interfaces between Smc3 and Rad21 are covalently linked (Eichinger *et al*, 2013). This covalent fusion promotes cohesin stability by preventing WAPL-mediated release and was previously shown to induce moderate defects in wing morphology (Ribeiro *et al*, 2016; Fig 5A). The resulting defects were more severe if this fusion is expressed with concomitant depletion of Lds

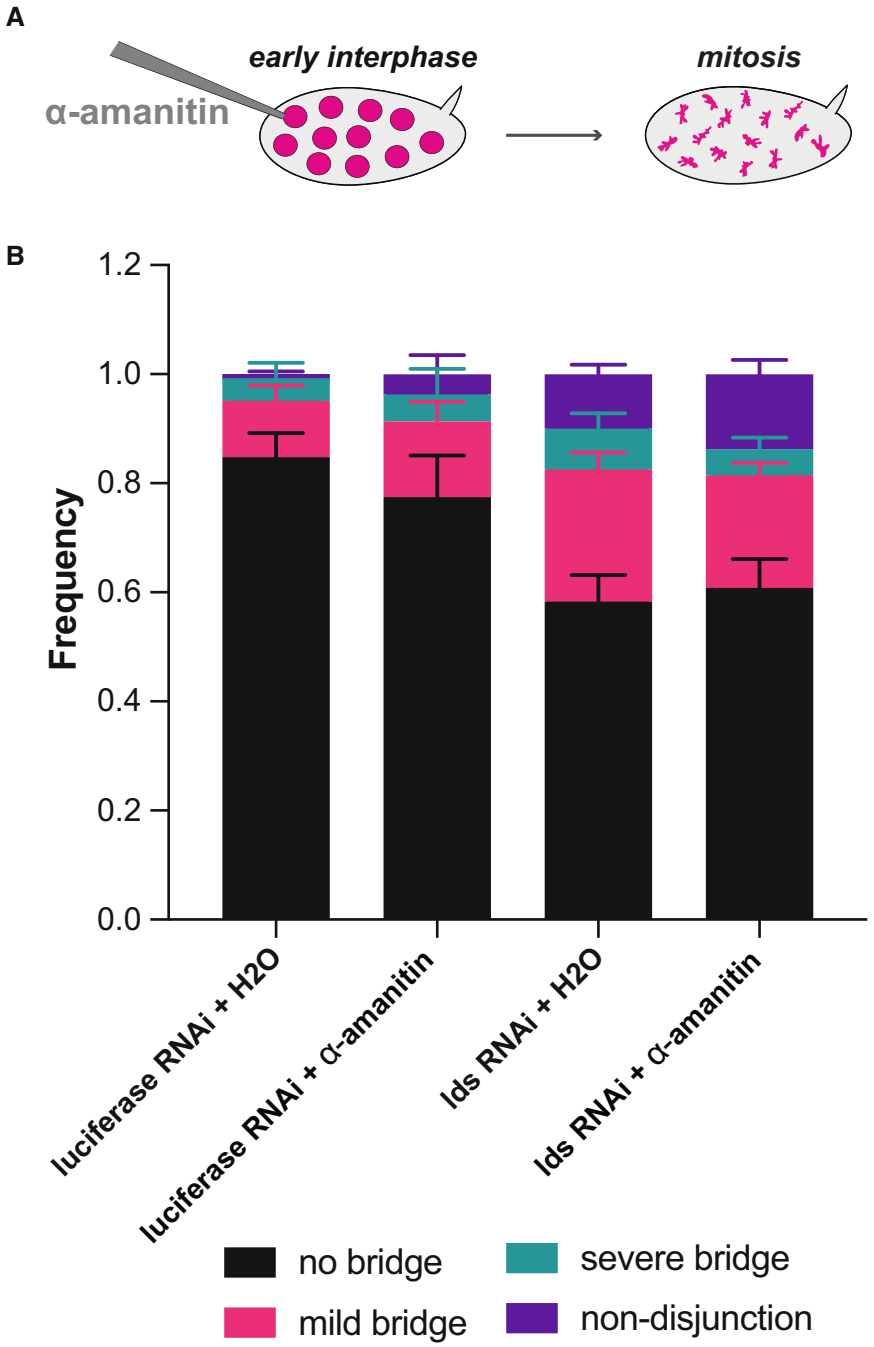

Figure 4. Transcription inhibition is insufficient to restore mitotic fidelity in Lds-depleted embryos.

A Schematic representation of the experimental layout: luciferase/lds-depleted embryos were microinjected with water or alpha-amanitin (1 mg/ml) in late mitosis/early interphase. Transcription levels were monitored during the following interphase (Fig EV4) and segregation defects in the subsequent mitosis (B).

B Segregation defects upon inhibition of transcription in luciferase and lds RNAi. Graph depicts mean ± s.e.m. of the frequencies of defects scored in 11 (luciferase RNAi, H_2O and lds RNAi, α-amanitin) or 8 (lds RNAi, H_2O and Luc RNAi, α-amanitin) independent embryos; a total of ~800 nuclei were scored per condition.

Source data are available online for this figure.

(Fig 5A). Similarly, co-depletion of Lds was also an effective enhancer of the defects associated with the impaired removal of DNA–DNA catenations, including RNAi for the condensin subunit Cap-D2 and RNAi for Top2 (Fig 5A).

These findings support the hypothesis that Lds is involved in the efficient resolution of sister chromatids. To distinguish whether it works through the release of cohesin and/or DNA catenations, we first monitored the dynamics of the cohesin removal in the presence

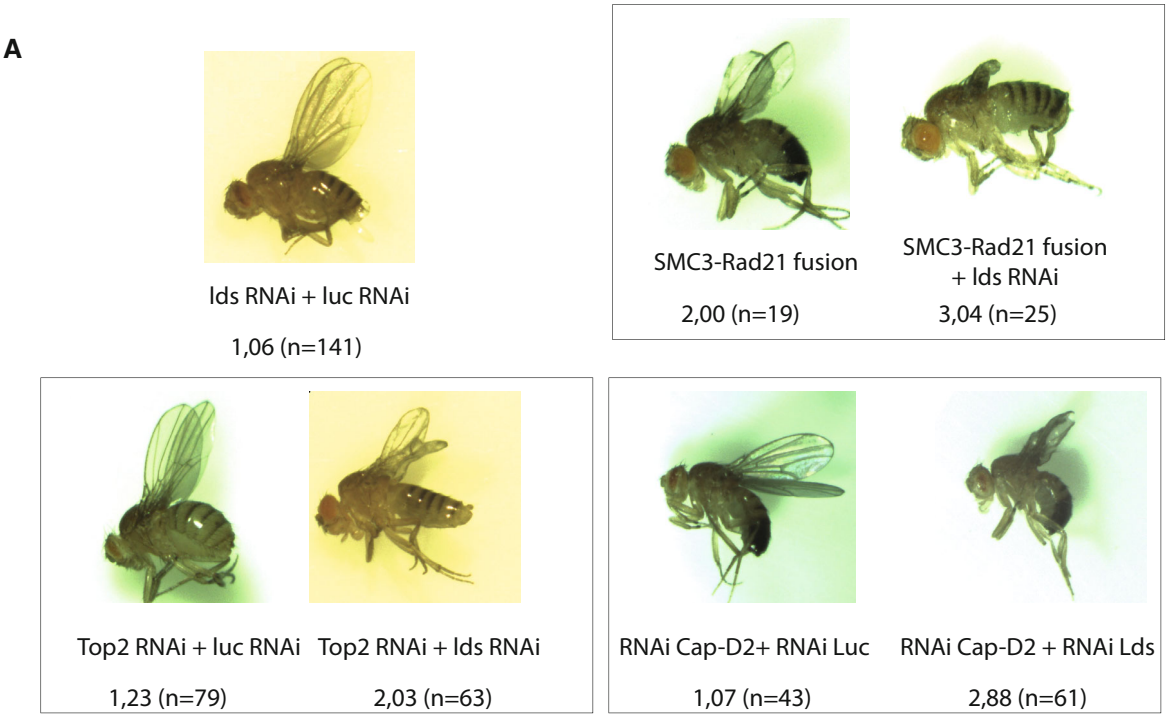

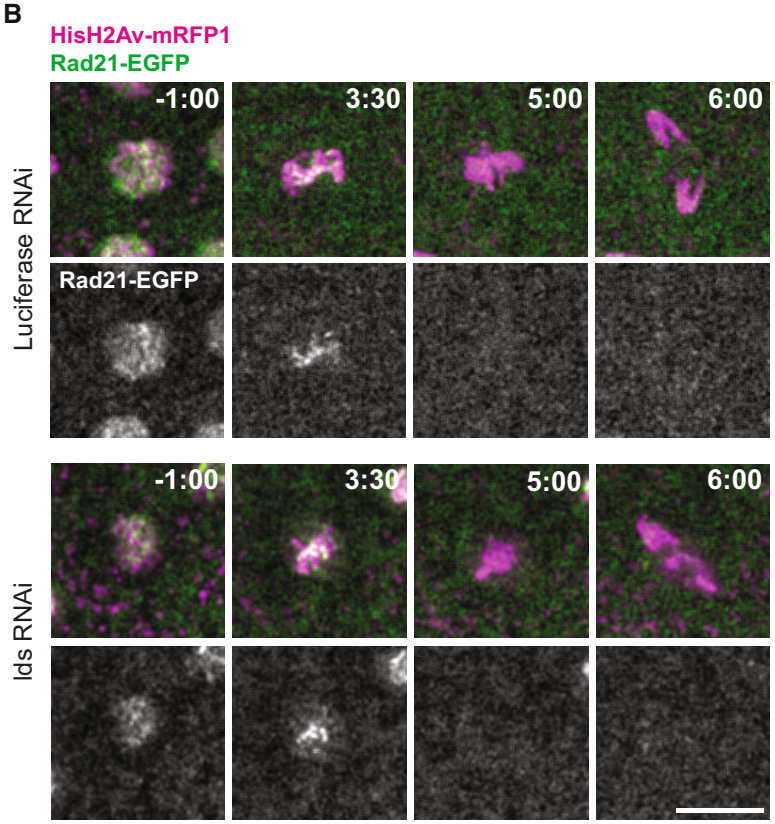

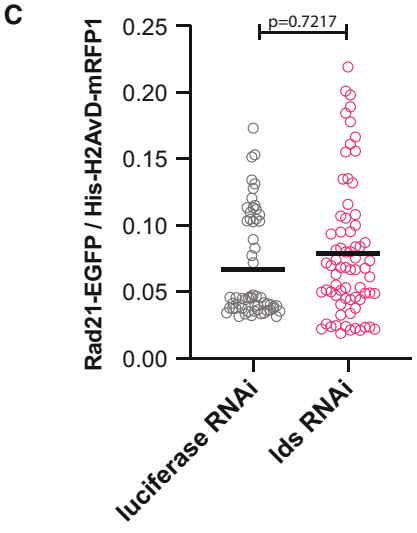

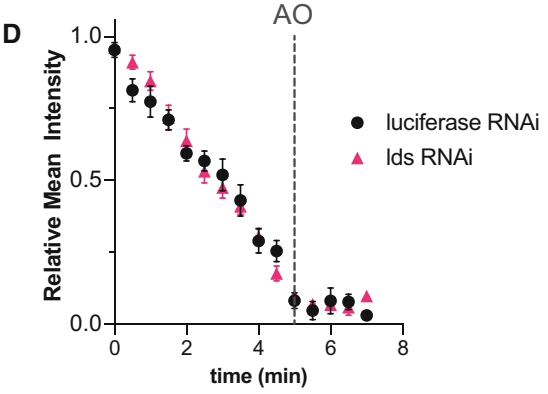

Figure 5.

Figure 5. Lds genetically interacts with various players in sister chromatid resolution but does not control cohesin levels in mitosis.

A Wing morphology phenotype obtained upon depletion of Lds combined with control co-depletion (luciferase RNAi) or expression/depletion of chromosome architecture modulators. Wing morphology defects were classified according to their severity (1 = normal wings and 5 = no wing); depicted numbers indicate the average morphology grade and the number of flies counted, from at least two independent experiments.

B Live-cell imaging analysis of the kinetics of Rad21-EGFP (green) removal from mitotic chromosomes in luciferase- and lds-depleted embryos. DNA is marked with H2AvD-mRFP1 (magenta); times are relative to NEBD; scale bar is 10 μm and applies to all images.

C Quantification of the mean fluorescence intensity of Rad21-EGFP, normalised to the mean intensity of HisH2AvDmRFP1, measured 5 min before anaphase onset, in luciferase/lds-depleted embryos. Each dot represents a single metaphase and black lines the mean. luciferase RNAi, $n = 5$ embryos, 59 metaphases; lds RNAi $n = 5$ embryos, 71 metaphases; Statistical analysis was performed using nested two-tailed t-test.

D Kinetics of Rad21-EGFP disappearance from chromatin in luciferase and lds-depleted embryos. Mean fluorescence intensity of Rad21-EGFP within the chromosomal area was normalised to the mean intensity of HisH2AvDmRFP1. Measurements of individual nuclei were aligned based on the time of anaphase (when sister chromatid separation could be observed, t = 5), and normalised to the maximum value within each dataset. Each symbol represents mean ± s.e.m. of 15 metaphase (from five independent embryos) per experimental condition.

Source data are available online for this figure.

or absence of Lds. These results revealed that upon depletion of Lds, and similarly to control strains, the cohesin kleisin subunit Rad21-EGFP was mainly detected at the centromeric regions and not along chromosome arms (as observed upon WAPL removal; Oliveira *et al*, 2014; Fig 5B). Moreover, we could not detect any change in overall chromatin levels of Rad21-EGFP upon lds depletion (Fig 5C). These findings confirm that the removal of cohesin complexes along chromosome arms is unperturbed. Additionally, we could not detect any delay in the kinetics of centromeric Rad21-EGFP removal at the metaphase to anaphase transition (Fig 5B and D), supporting an efficient Separase-mediated cleavage of cohesin. Altogether, these results support that Lds does not enhance or stabilise cohesin complexes on DNA in a way that could potentially preclude the efficient removal of cohesin-mediated linkages. Conversely, depletion of WAPL or cohesin does not perturb the localisation of Lds (Fig EV5), suggesting that Lds activity may be independent of cohesin regulation.

We thus focussed on investigating how Lds could contribute to the removal of DNA catenations, either directly or via interaction with other modulators. We first probed for the presence of Condensin I and Top2 on mitotic chromosomes upon Lds removal. We used strains expressing endogenously tagged Barren-EGFP (Kleinschnitz *et al*, 2020) and Top2-EGFP (developed here, see Materials and Methods). In both cases, we found that Top2-EGFP and Barren-EGFP were efficiently recruited to mitotic chromosomes (Fig 6A–D), indicating that Lds is not required for the chromatin targeting of these critical players in chromosome resolution. Interestingly, we observed an enrichment of both Top2 and Condensin I subunit Barren at the site of the anaphase bridges observed upon depletion of Lds (Fig 6A, C, E and F). These findings imply that DNA bridges caused by lds knockdown retain the machinery responsible for DNA resolution. Reciprocally, we find that DNA bridges that result from improper sister chromatid resolution induced by other perturbations (e.g. mild RNAi for the condensin I subunit Cap-D2 or the cohesin destabiliser wapl) retain high levels of Lds at the bridge site, as evidenced by the increased amount of Lds-EGFP in those regions (Fig 6G and H). These results suggest that the bridges observed upon Lds loss are likely caused by unresolved DNA catenations, resulting in the hyper-recruitment of their resolution machinery at mitotic exit. Interestingly, the presence of Lds on chromatin bridges caused by other means suggests that Lds is by itself part of this resolution mechanism.

To further test a potential cooperation between Lds and the primary enzyme responsible for DNA decatenation, Top2, we sought to probe for a possible interplay between these two proteins on mitotic chromatin. For this, we established conditions to trap Top2 on mitotic chromatin artificially: embryos were microinjected with $UbcH10^{DN}$ to induce metaphase arrest (Oliveira *et al*, 2010) and subsequently microinjected with the Top2 inhibitor ICRF-193 (Fig 7A). Under these conditions, we observed a sharp increase in the amount of Top2-EGFP detected, despite the overall decompaction of mitotic chromatin (Fig 7B). We then used the same assay to monitor the

Figure 6. Lds localises to DNA bridges.

A–F (A, C) Chromatin localisation of chromosome assembly factors (Top2 (A) and Condensin I subunit Barren (C), in green) upon RNAi for luciferase (left) or lds (right) in early embryos. DNA is marked with H2AvD-mRFP1 (magenta); scale bars are 10 μm and apply to all images. (B, D) Quantification of the mean fluorescence intensity of Top2-EGFP (B) or Barren-EGFP (D), normalised to the mean intensity of HisH2AvDmRFP1, measured 2–3 min before anaphase onset, in luciferase/lds-depleted embryos. Each dot represents a single metaphase and black lines the mean. B: luciferase RNAi, $n = 11$ embryos, 301 metaphases; lds RNAi $n = 6$ embryos, 177 metaphases; D: luciferase RNAi, $n = 5$ embryos, 171 metaphases; lds RNAi $n = 5$ embryos, 134 metaphases. Statistical analysis was performed using nested two-tailed t-test. (E, F) Quantification of telophase figures with and without enrichment of Top2-EGFP (E) or Barren-EGFP (F) at the bridge site; frequency of cells with no bridge or nondisjunction are also shown. Graphs represent the mean ± s.e.m. of 12 (luciferase RNAi) and 10 (lds RNAi embryos) for Top2-EGFP and 7 (luciferase RNAi) and 12 (lds RNAi embryos) for Barren-EGFP. An average of 40 telophases was scored per embryo.

G Telophase images of embryos depleted for luciferase (left), Cap-D2 (middle) and wapl (right) RNAi, and expressing Lds-EGFP (green) and HisH2AvDmRFP1 (magenta). Bottom panels depict Lds-EGFP alone. Scale bar is 10 μm and applies to all images.

H Quantification of telophase figures with and without enrichment of lds-EGFP at the bridge site, in the referred conditions; frequency of cells with no bridge or nondisjunction are also shown. Graphs represent the mean ± s.e.m. of 9 (luciferase RNAi) and 12 (Cap-D2 RNAi) or 10 (Wapl RNAi) embryos. An average of 45 telophases was scored per embryo.

Source data are available online for this figure.

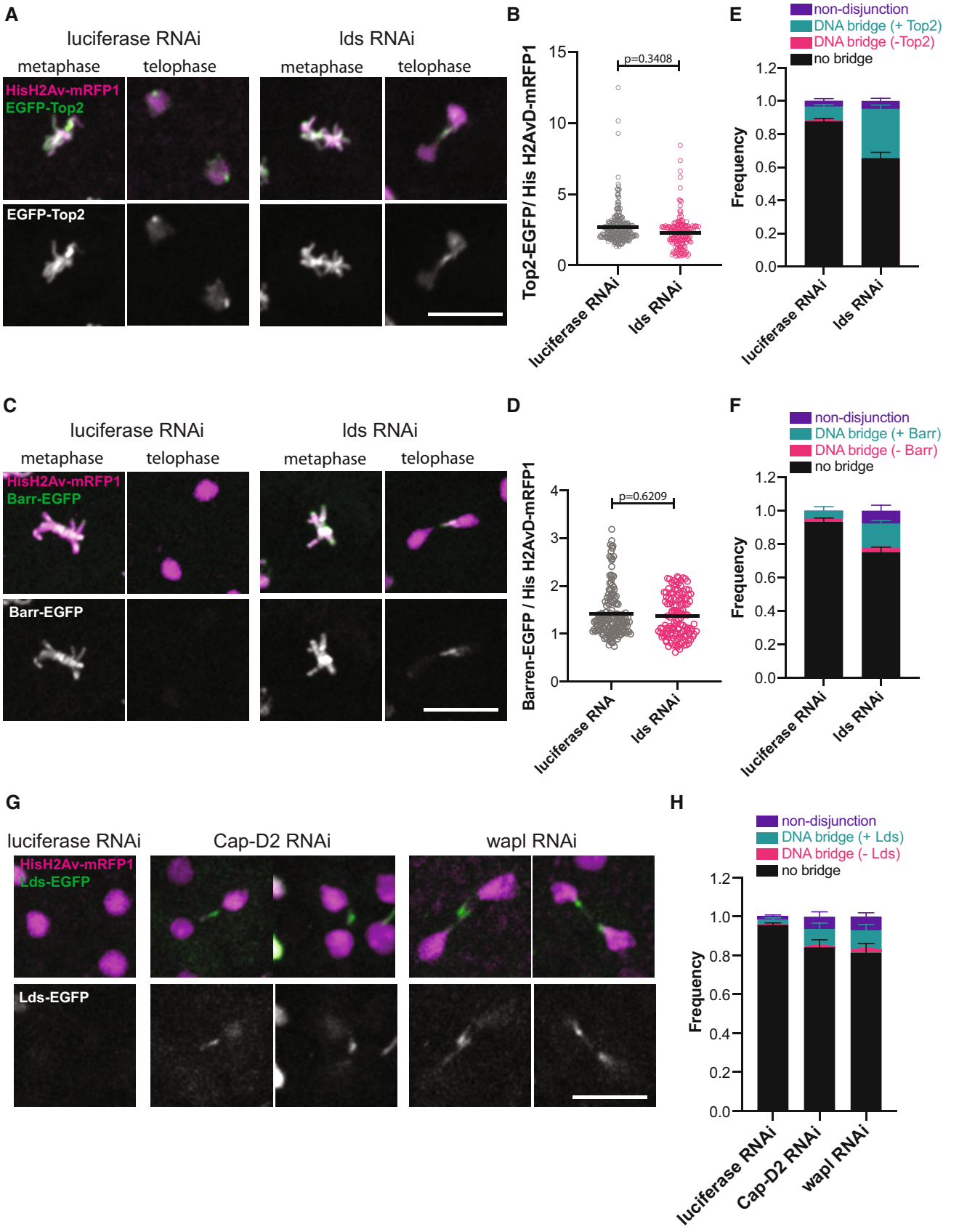

Figure 6.

behaviour of Lds-EGFP upon Top2 inhibition. We found that upon ICRF-193 injection, there was a sharp increase in chromosome-bound Lds-GFP levels (~ 2.5 fold) (Fig 7C). Notably, the rise in Lds-GFP does not follow the same kinetics of Top2. It increases faster than Top2 itself, reaching a steady state after this initial raise. These findings imply that Lds' chromatin targeting is sensitive to Top2 inhibition.

To further evaluate the dependence of Lds' chromatin binding on Top2 inhibition, we monitored the dynamic behaviour of both proteins using fluorescence recovery after photobleaching (FRAP) with and without ICRF-193 treatment (Fig 7D). For this analysis, the fluorescence of an entire metaphase plate was bleached, and the fluorescence recovery was subsequently monitored. This analysis revealed that Top2 displays a highly dynamic association with chromatin ($t_{1/2}$ = 36.6 ± 10.8 s), in accordance with previous reports (Christensen *et al*, 2002; Tavormina *et al*, 2002; Fig 7E). A similar analysis on Lds demonstrates that Lds-EGFP displays a comparable dynamic turnover ($t_{1/2}$ = 32.4 ± 5.7 s; Fig 7F). Importantly, we observed that treatment of ICRF-193 increased the half-time of Top2 recovery significantly ($t_{1/2}$ = 4.43 ± 1.51 min, $P < 0.0001$ One-way ANOVA, Fig 7E), evidencing the differential mode of binding of this molecule to chromatin in the presence of the inhibitor. In contrast, Lds retains its high turnover rate ($t_{1/2}$ = 40.14 ± 8.94 s), indicating it is not co-trapped with Top2 on chromosomes upon ICRF treatment (Fig 7F). Altogether, these results suggest that Lds is likely sensitive to changes in the DNA molecule induced by Top2 inhibition, which may aid in the efficient resolution of sister chromatid intertwines.

Lds has a dual function in mitosis

Considering the dual role observed for Lds on mitotic transcription termination and sister chromatid resolution, we next asked whether these two functions are interdependent or represent two distinct actions required during mitosis. To address this, we probed whether transcript release depends on Top2 activity. We monitored the time of MCP-labelled transcript disappearance from chromatin, in situations of impaired Top2, achieved by microinjection of the Top2 inhibitor ICRF-193 before mitotic entry. This treatment resulted in a significant increase in the MCP-EGFP signals in both luciferase and lds RNAi, possibly due to transcription stalling caused by Top2 inhibition/trapping (Fig 8A–C). However, ICRF-193 injection does not change the timing of transcript release, and a significant delay is solely detected in the absence of Lds, independently of the Top2 activity state (Fig 8A and D). These results imply that Top2 activity is not required for efficient transcriptional termination in these embryos.

Discussion

Here, we uncovered the depletion of lds as a strong suppressor of the defects associated with cohesion loss. We showed that Lds contributes to mitotic fidelity, as a dual-function chromatin factor: it ensures prompt transcription termination and efficient sister chromatid resolution. We further show that removal of mitotic transcripts from chromatin does not rely on Top2 strand passage activity or efficient chromosome decatenation. These findings suggest that Lds may modulate mitotic chromatin to facilitate both processes. Notably, cohesin has also been involved in these two activities, which can explain the suppressor effect on wing morphology. Specifically, the presence of cohesin is known to preclude efficient sister chromatid resolution, possibly by keeping sisters in such proximity that favours sister chromatid intertwining as opposed to their resolution (Farcas *et al*, 2011; Sen *et al*, 2016). Cohesin retention is also required and sufficient for active transcription on mitotic chromosomes (Perea-Resa *et al*, 2020). Hence, our findings uncovered unprecedented links between these two processes that reshape chromatin during mitosis both at the structural and functional levels.

Classic views have postulated that mitotic transcription inhibition (MTI) would be a passive consequence of mitosis, either due to changes in chromosome organisation and/or by biochemical changes imposed by the rise in cdk1 activity (Gottesfeld & Forbes, 1997). In contrast with these dogmas, our results, together with other studies (Jiang *et al*, 2004; Liang *et al*, 2015; Perea-Resa *et al*, 2020; Sharp *et al*, 2020), suggest that MTI is driven by an active mechanism that ensures prompt transcriptional shutdown upon mitotic entry. Note that in the absence of Lds, chromosomes can still condense and progress through mitosis with regular timings (or with slight delays). These findings imply that transcripts can remain engaged with mitotic chromatin despite the chromosomal compaction and high Cdk1 activity. Collectively, these findings support that MTI is a more active and regulated process than previously anticipated.

The need for dedicated machinery to support such mechanisms may have evolved to facilitate mitotic progression. A tempting hypothesis is that pervasive transcription can compromise mitotic fidelity. Indeed, some evidence refers to increased mitotic defects

Figure 7. Lds chromatin association is sensitive to Top2 inhibition.

A Schematic representation of the experimental layout.

B, C Loading of EGFP-Top (B) and Lds-EGFP (C) (labelled in green) on mitotic chromatin of metaphase-arrested embryos (UbcH10^{C114S} injection), upon subsequent injection of DMSO/ICRF-193; DNA is marked with H2AvD-mRFP1 (magenta); times (min:sec) are relative to time of injection. Graphs depict integrated intensities normalised to the first time point, represented as mean (dots) ± SD (grey area); n = 54 (Lds + ICRF-193, Lds + DMSO, Top2 + ICRF-193) or 47 (Top2 + DMSO), derived from 8 to 9 independent embryos per experimental condition.

D Schematic representation of the experimental layout.

E, F FRAP analysis with and without ICRF-193 treatment for EGFP-Top2 (E) and Lds-EGFP (F). Metaphase-arrested embryos were microinjected with DMSO/ICRF-193 and an entire metaphase plate was bleached 10 min after. Graphs depict recovery of fluorescence signal over time. Dots represent average and grey areas SD; Top2: n = 14 (DMSO) and 18 (ICRF-193) metaphases; Lds: n = 11 (DMSO) and 9 (ICRF-193) metaphases, derived from 3 to 7 independent embryos per experimental condition.

Data information: Scale bar is 10 μm and applies to all images.
Source data are available online for this figure.

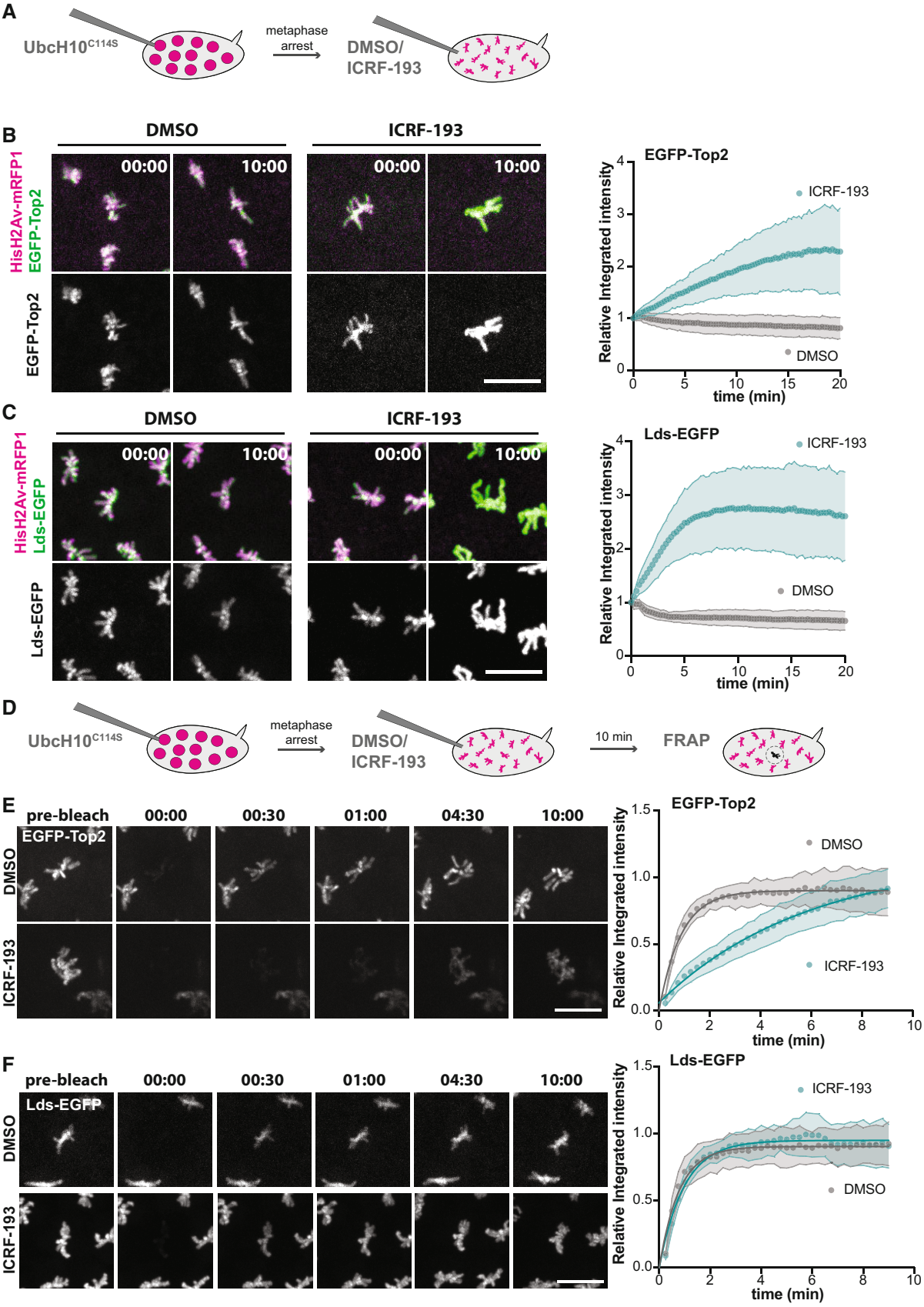

Figure 7.

upon chronic perturbation of putative MTI players, although these defects have never been analysed in great detail. For example, RNAi for TTF2 or Gdown1 leads to an increase in the presence of binucleated cells or p53 activation after aberrant mitosis (Jiang *et al*, 2004; Ball *et al*, 2022), whereas impairment of PolII clearance through P-TEFb removal leads to delays in the progression of cell

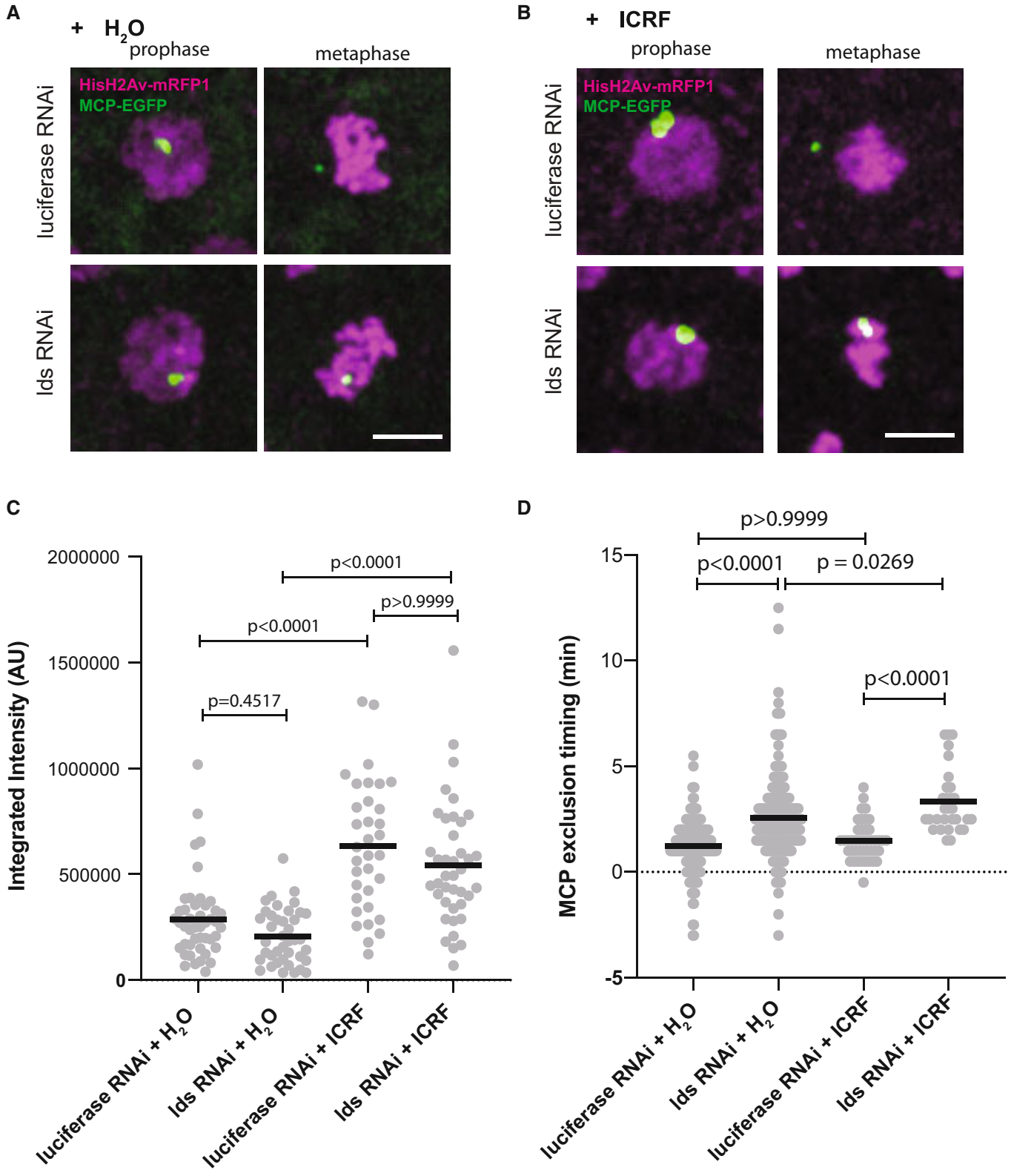

Figure 8.

Figure 8. Top2 is dispensable for timely release of mitotic transcripts from chromatin.

A, B Representative images of mitotic nuclei in prophase (1 min before NEBD) and metaphase (1 min before anaphase onset), upon RNAi for luciferase/lds, microinjected with water (A) or ICRF-193 (B). Scale bars are 5 μm and refer to all images.

C Integrated intensity for the MCP-EGFP signal measured 1 min before nuclear envelope breakdown with and without ICRF-193 injection. Sample size: luciferase RNAi + H_2O $n = 45$ nuclei from seven independent embryos; lds RNAi + H_2O $n = 40$ nuclei from eight embryos; luciferase RNAi + ICRF $n = 34$ nuclei from 7 embryos; lds RNAi + ICRF-193 $n = 40$ nuclei from 8 embryos. Statistical analysis was performed using Kruskal–Wallis test, using Dunn's test for multiple comparisons.

D Time (min) of disappearance of the MCP-EGFP signal from chromatin in the referred conditions, relative to NEBD; $n = 196$ (luciferase RNAi + H_2O), 205 (lds RNAi + H_2O), 43 (luciferase RNAi + ICRF) and 30 (lds RNAi + ICRF-193) nuclei, derived from at least three independent embryos per experimental condition. Statistical analysis was performed using the nonparametric Kruskal–Wallis test and Dunn's test for multiple comparisons.

Source data are available online for this figure.

division (Liang *et al*, 2015). Ectopic retention of SAF-A–RNA complexes on mitotic chromosomes leads to defects in metaphase chromosome congression (Sharp *et al*, 2020). Furthermore, the mitotic defects observed upon WAPL depletion could be rescued upon transcription inhibition, arguing that most defects associated with WAPL loss are caused by transcription-mediated events (Perea-Resa *et al*, 2020). In the present work, although transcription inhibition does not rescue the frequency of mitotic defects after depletion of Lds, it is still possible that pervasive transcription perturbs mitotic fidelity, although to a minor extent compared with defects caused by defective sister chromatid resolution. In *Drosophila* syncytial blastoderm embryos, transcription levels are low, restricted to the minor wave of zygotic gene activation (Pritchard & Schubiger, 1996). Conversely, topological issues are expected to be high due to the extremely fast genome replication. Hence, it is conceivable that in this particular system, errors in mitosis after depletion of Lds are mostly caused by decatenation defects rather than impaired transcription termination or pervasive transcription. The synergy between the emerging players in MTI as participants in other functions in chromosome architecture and/or transcriptional control, as illustrated in the present study, brings an additional challenge to the understanding of how transcription termination defects impair mitotic fidelity, and the mechanistic understanding of this interference remains unknown.

The uncovered link between sister chromatid resolution and mitotic transcript eviction reported here raises intriguing questions on how these two combined systems may have evolved and specialised across the tree of life. In mammalian cells, another SNF2 helicase-like protein, Plk1-interacting checkpoint helicase (PICH), has been documented to aid in sister chromatid resolution during anaphase by cooperating with Top2 and Top3 (Baumann *et al*, 2007; Spence *et al*, 2007; Pitchai *et al*, 2017). *Drosophila* does not have a true PICH orthologue. Lds and PICH share very low homology, except for the conserved helicase-like domains, common to the entire SNF2-like family (e.g. Lds does not have TPR domains, known to promote binding to its co-factor BEND3; Pitchai *et al*, 2017). Moreover, PICH is found mainly in the centromeric region (Baumann *et al*, 2007), whereas we see Lds located all over chromosomes in *Drosophila* embryos. However, it is possible that in *Drosophila*, Lds shares the function of both PICH and TTF2, the latter known to participate in mitotic transcription termination in human cells (Jiang *et al*, 2004), which have diverged in mammalian systems.

It also remains to be established how Lds can perform both functions at the mechanistic level, but it is conceivable that both the removal of nascent mRNAs and sister chromatid resolution rely on common mechanistic principles. In line with what has been observed for other SNF2-like proteins (Durr *et al*, 2006), Lds may induce helical torsion on DNA which could drive Pol II eviction, consistent with its transcription termination activity identified *in vitro* (Xie & Price, 1996, 1998). The sudden recruitment of Lds upon mitotic entry may trigger global premature transcription termination (i.e. abortion). These changes in DNA organisation may concomitantly favour substrate recognition by Top2. Lds may thus be a previously unknown player in ensuring proper directionality to Top2 reactions, which is essential for efficient genome partitioning (Piskadlo & Oliveira, 2017). Further studies are required to establish how Lds acts on mitotic chromatin to impose this dual outcome.

Materials and Methods

Fly strains

Drosophila melanogaster flies were raised at 25 or 18°C in polypropylene vials containing standard fly food. Transgenic flies expressing EGFP-Top2 or Lds-EGFP were obtained by CRISPR-mediated mutagenesis, performed by WellGenetics Inc., using modified methods of (Kondo & Ueda, 2013). In brief, gRNA sequences GTACATCTGTTCGATGGACA[GGG] (Top2) or GGCGCCTGTAAGG ACACCAT[CGG] (lds) were cloned into U6 promoter plasmid(s). Cassette EGFP containing EGFP and two homology arms were cloned into pUC57-Kan as donor template for repair. *CG10223* or *lds/CG2684*-targeting gRNAs and hs-Cas9 were supplied in DNA plasmids, together with donor plasmid for microinjection into embryos of control strain *w[1118]*. F1 flies were screened by PCR and further validated by genomic PCR and sequencing. CRISPR generates a break upstream of *CG10223/top2 or* downstream of *lds/ CG 2684* and is replaced by cassette EGFP.

All other strains used in this study were previously described and are summarised in Table 1.

Embryo viability scoring

To measure embryo viability for each condition, equal numbers of flies (virgin females and males) were placed in fly cages with apple juice agar plates. The agar plates were collected after 24 h, and the number of embryos was scored. After 48 h, the number of hatched larvae in each plate was counted. Three replicates were done for each condition. For the rescue experiments, a similar approach was used but embryos were allowed to develop on the coverslips placed onto fly food, after mRNA microinjection, and hatched embryos were determined by the presence of an empty eggshell.

Table 1. Genotype of the fly strains used in this study.

#CHR lab internal reference	Genotype	Reference/Source
1881	*w*;; lds-EGFP CRISPR[EGFP]* (Lds-EGFP)	This study
1882	*w^{1118}; EGFP-CG10223 CRISPR [EGFP]/CyO* (EGFP-gTop2)	This study
1883	*w*; Rec(EGFP-CG10223 CRISPR [EGFP], HisH2AvD-mRFP1)/CyO;*	This study (recombined from CHR#1882 and BDSC#23651, Schuh *et al* (2007))
1893	*w*; HisH2AvD-mRFP1; lds-EGFP CRISPR[EGFP]*	This study (derived from CHR#1881 and BDSC#23651, Schuh *et al* (2007))
1892	*w*;If/CyO;{w[+mC]=GAL4::VP16-nos.UTR}1C* (nosGal4)	Derived from BDSC #64277, Doren *et al* (1998)
1890	*w*;P(nub-GAL4.K)2;MKRS/TM6,B* (nub-Gal4)	Derived from BDSC #86108, Ng *et al* (1996), Wu & Cohen (2002)
1891	*y^1 sc* v^1 sev^{21}; Ply[+t7.7] v [+t1.8]=TRiP.HMS01389 lattP2* (lds RNAi)	BDSC # 34980
na	*y^1 sc* v^1 sev^{21}; P(y[+t7.7] v [+t1.8]=VALIUM20-mCherry) attP2* (mCherry RNAi)	BDSC # 35785
1889	*y^1v^1; P(y[+t7.7] v[+t1.8] =TRiP.JF01355)attP2* (luciferase RNAi)	BDSC # 31603
1276	*w^{1118};UAS-san RNAi(P (KK101696)VIE-260B)/CyO*	VDRC # 180610
	w^{1118}; nubbin-Gal4, UAS-san RNAi(P(KK101696)VIE-260B)/ CyO	Ribeiro *et al* (2016)
1888	*y^1v^1; P(y[+t7.7] v[+t1.8]= TRiP.JF01280)attP2* (Cap-D2 RNAi)	BDSC #31478
1751	*y^1v^1; P(y[+t7.7] v[+t1.8]= TRiP.JF01300)attP2* (Top2 RNAi)	BDSC #31342
1894	*y[1] sc[*] v[1] sev[21]; P{y [+t7.7] v[+t1.8]= TRiP.HMS05805}attP40* (wapl RNAi)	BDSC #67892
1895	*y[1] sc[*] v[1] sev[21]; P{y [+t7.7] v[+t1.8]= TRiP.HMS00272}attP2* (SA1 RNAi)	BDSC #33395
1896	*w*;P(nub-GAL4.K)2; Lds-EGFP CRISPR[EGFP]/TM6,B*	This study
1897	*w*; If/CyO; Lds-EGFP CRISPR [EGFP], lds RNAi/TM6,B*	This study
1898	*w*; If/CyO; Lds-EGFP CRISPR [EGFP], luciferase RNAi/TM6,B*	This study
1899	*w*; HisH2AvD-mRFP1;Rec ({w [+mC]=GAL4::VP16-nos.UTR}1C, Lds-EGFP CRISPR[EGFP])/TM6,B*	This study
1398	*w*;P(UAS-Smc3-Rad21-EGFP)*	Eichinger *et al* (2013)
1152	*w*;P(tubpr-Rad21(wt)-EGFP)*	Oliveira *et al* (2014)
	w; Barr-EGFP CRISPR[EGFP]/ CyO;*	Kleinschnitz *et al* (2020)
1884	*y[1] w[*]; P{w[+mC]=nos-MCP.EGFP}8; nosGal4*	Derived from Garcia *et al* (2013)
1885	*y[1] w[*]; P{hbP2-MS2-lacZ} JB38F*	Garcia *et al* (2013)
1560	*w; $Barr^{L305}$/ Df(2L)Exel7077; Barr(175 - 3TEV)-myc10 III.5*	Piskadlo *et al* (2017)
1886	*w*; Rec (nos-MCP.EGFP, Df(2L) Exel7077, HistH2AvD-mRFP1);;*	This study
1900	*w[*]; PBac{y[+mDint2] w[+mC]= eveBAC-MS2-y}VK00033*	BDSC #92368 Berrocal *et al* (2020)
1901	*w[*];;[pbphi-sna shadow enhancer-sna primary enhancer-sna promoter-24x MS2-lacZ-24x PP7-αTubulin 3'UTR]*	Fukaya *et al* (2017)

Western blot

Embryos were collected for 2.5 h and dechorionated in 50% bleach for 2 min. After copious washes with water, 30 embryos from each condition were manually selected, needle punctured, and the resulting lysate was resuspended in 1× Laemmli buffer and boiled for 5 min at 95°C. Samples were loaded onto a 7.5% SDS gel and transferred to a nitrocellulose blot membrane. Western blot analysis was performed according to standard protocols using the following antibodies: anti-GFP (1:750, Roche, Cat# 11814460001, RRID:AB_390913) and anti-α-tubulin (Santa Cruz, 1:5000, Cat #sc-53030, RRID:AB_784594).

Microinjections

Embryos were prepared for imaging and microinjected as previously described (Carmo *et al*, 2019), except for 5-EUTP incorporation and mRNA injections to score embryonic viability, for which we followed a protocol that enables microinjections prior to chorion removal (Gompel & Schröder, 2015). Embryos were then microinjected with proteins/drugs at the following concentrations: alpha-amanitin (1 mg/ml), $UbcH10^{C114S}$ (prepared as in Oliveira *et al*, 2010, at ~30 mg/ml); ICRF-193 (280 μM); mRNA for RNAi-resistant lds (1 mg/ml; prepared using mMESSAGE mMACHINE T3 transcription kit (Thermo Fisher), using Lds ORF subcloned in pRNA vector, after site-directed mutagenesis to replace the RNAi target sequence "CCGGCTCAATCTGCTAATGAA" by "TAGGCTGAACCTTCTGATGAA"); 5-ethynyl-uridine-5′-triphosphate (5-EUTP) (10 mM, Abcam #ab146744-25ul) in RNase-free water.

Microscopy

Imaginal discs and early embryos were prepared for live-cell imaging as previously described (Silva *et al*, 2018; Carmo *et al*, 2019). All time-lapse movies of live embryos/wing discs (except Rad21-

EGFP imaging) were obtained using Confocal Z-series stacks with a Yokogawa CSU-X Spinning Disk confocal, mounted on a Leica DMi8 microscope, with a 63× 1.3NA glycerine immersion objective (except for imaging of Lds-EGFP total levels in wing discs (Fig EV1A), performed with a 20× dry NA 0.8 objective), using the 488 nm and 561 nm laser lines and an Andor iXon Ultra EMCCD 1024 × 1024 camera. The system was controlled with Metamorph software (Molecular Devices). For imaging of Rad21-EGFP and DNA FISH embryos, confocal Z-series stacks were acquired on a Andor Dragonfly Spinning Disk confocal, mounted on a Nikon Ti2 microscope, with a 60× 1.2 NA water immersion objective, using the 405, 488 nm and 561 nm laser lines and a Andor Sona sCMOS 4 MPix camera using a 1,600 × 1,350 FOV.

Quantitative imaging analysis

For image analysis, z-stacks were max-intensity projected using FIJI. Mitotic errors were manually evaluated based on H2AvDmRFP1 signals. Cells where segregation fidelity could not be assigned were excluded from the analysis. Times of anaphase and transcript eviction were measured relative to nuclear envelope breakdown, defined by the time chromatin signal loses its round organisation. Transcript removal time was defined by the time MCP-EGFP labelled reporter transcripts were either no longer detected or observed outside the chromosomal region.

For quantitative analysis of MS2 signal decay (Fig EV3C), images were max projected and bleach corrected (FIJI). A fixed-size ROI (10 pixel diameter) was placed around the MCP-EGFP signal. Mean fluorescence intensity was measured over time, subtracted to the mean fluorescence of the cytoplasmic signal and normalised to the maximum value within each dataset. Individual measurements were aligned based on the time of NEBD.

For quantitative analysis of MCP-EGFP levels before/after alpha-amanitin injection (Fig EV4C and D), MCP-EGFP signal was first segmented based on the Hist-H2AvD-mRFP1 signal, to select for chromosomal area. An automatic threshold was defined 1 min before NEBD and integrated fluorescence intensities above the defined threshold were measured.

For quantitative analysis of Top2-EGFP/Barren-EGFP levels (Fig 6), we used embryos undergoing mitosis 10–12. Max projections were bleach corrected and background subtracted. Metaphase area was defined based on HisH2AvD-mRFP1, and the mean fluorescence intensity of both channels was measured per metaphase.

Scoring of the enrichment of Top2-EGFP/Barren-EGFP/Lds-EGFP at chromatin bridges was performed manually. Enrichment was defined when the levels of the protein of interest at the bridge site were higher than HisH2AvD-mRFP1, compared with other chromosomal regions.

For quantitative analysis of chromatin-bound levels of Top2/Lds (Fig 7), images were max projected, background subtracted, and Gaussian blurred (FIJI) and cropped for individual metaphases. ROIs were selected based on segmentation of the Histone mRFP1 channel, using automatic Huang threshold, to select for chromosomal area. Integrated intensities were measured for each ROI in either Lds/Top2 and normalised to the first time point.

When possible, specific measures were used to reduce subjective bias, including random selection of analysed nuclei, and blinding during quantification.

Early zygotic genes RNA labelling

Labelling of recently transcribed RNAs was performed as in Cho *et al* (2022) with minor modifications. Embryos were collected for 2–2.5 h and prepared/microinjected as described above. After 5-EUTP injection, embryos were allowed to incorporate 5-EUTP for 20–40 min and then dechorionated in 50% bleach for 2 min. Embryos were fixed with a 1:1 mixture of heptane and 37% formaldehyde (4 ml each), with vigorous shaking for 1 min and additional 10 min standing at room temperature. Formaldehyde was removed and replaced by equal volume of methanol and shacked for 1 min. Heptane was removed, and then, fresh methanol was added until the embryos sank from the interface to the bottom. Fixed embryos were stored in methanol at −20°C.

Fluorescent labelling of 5-EUTP was performed using Click-iT RNA Alexa Fluor 488 (Invitrogen, Cat# C10329). Fixed embryos were 4× washed and rehydrated with PBST for 5 min. The "click" reaction was then performed following the manufacturer's instructions for 30 min. Embryos were rinsed once with the Click-iT reaction rinse buffer, washed with 2× 10 min in PBST, and mounted on a glass slide in Dako (Agilent, Cat #S3023).

DNA FISH

Embryos were collected for 2–2.5 h, dechorionated in 50% bleach for 2 min and washed abundantly with water. Collected embryos were fixed as described above (see Early zygotic genes RNA labelling section) and stored at −20°C in methanol. Pooled embryos were rehydrated in a mixture of methanol:PBST (7:3, 1:1, and 3:7) for 3 min each and washed in PBST for 2 min. After, embryos were rinsed in 2× SSCT for 5 min and incubated in 2× SSCT-50% formamide for 5 min. Embryos were transferred to a PCR tube and incubated with 2× SSCT-50% formamide at 92°C for 5 min. At the same time, DNA probes were denatured (100 ng of each DNA probe – 5′-Alex594N-GAAAACATGAGGATCACCCATGTCTG-3′ and 5′-Alex594N-CAGACATGGGTGATCCTCATGTTTTC-3′ to label both DNA strands) in hybridisation buffer (20% dextran sulphate, 2×SSCT, 50% formamide and 0.5 mg/ml salmon sperm DNA) at 92°C for 5 min. Prehybridisation buffer was removed, and the DNA probe solution was added to the embryos. Embryos were incubated for 5 min at 92°C and overnight at 37°C in a thermocycler. The following day, embryos were washed with 2× SSCT for 5 min at room temperature, 2× SSCT warmed at 60°C for 10 min and again for 5 min at room temperature. Embryos were incubated with Hoechst (1:1,000 from a 1 mg/ml solution in SSC) for 30 min, protected from light. Embryos were mounted on a glass slide in DAKO.

Fluorescence recovery after photobleaching

FRAP analysis was performed in embryos from strains expressing solely the EGFP-tagged version of Lds or Top2 and HisH2AvDmRFP1 to monitor chromatin. Embryos were arrested in metaphase (UbcH10^{C114S}) and subsequently microinjected with DMSO/ICRF-193. FRAP analysis was performed 10 min after the second microinjection to allow for stabilisation of protein accumulation on chromatin. Four prebleach images were acquired every 15 s; 14 z-stacks 0.8 μm apart, followed by photobleaching of an entire metaphase with 1 pulse of 470 nm laser, using Andor's Mosaic

system (90% laser power). A total of 2–5 metaphases were bleached per embryo. Fluorescence recovery was monitored by subsequent imaging as described for prebleaching imaging. Quantitative analysis for fluorescence recovery for each metaphase was performed as above, measuring the integrated intensity of chromosomal regions (Hist-mRFP1-defined) over time, normalised to the image before bleach. Exponential curves were fit to a one-phase association equation $(Y = Y0 + (Plateau - Y0)^{*}(1 - \exp(-K^{*}x)))$ using GraphPad prism 9.0 to estimate half-times of recovery (K).

Experimental study design

All reported experiments have been independently replicated in the laboratory at least three times. No statistical methods were used to predetermine sample size. For experiments that rely on differential treatment (e.g. drug vs vehicle), embryos were randomly selected. The investigators were not blinded to allocation during experiments. For most, but not all, quantitative analysis, investigators were blinded to sample identify.

Statistical analysis

Statistical analysis was performed using GraphPad Prism 9.0. Standard statistical tests were employed, considering the normality of the samples (parametric/nonparametric). Standard adjustments were used for multiple comparisons. For cases of a large number of multiple observations from a single specimen (e.g. metaphase levels of a given protein), we used nested analysis to take into consideration the hierarchy of the observations. Details for each comparison can be found on the respective figure legends, and *P*-values are indicated in the respective graphs (the exact number, when precise calculation is possible, or upper limits).

Reagent availability

All reagents generated in this study will be distributed upon request.

Data availability

This study includes no data deposited in external repositories.

Expanded View for this article is available online.

Acknowledgements
We thank members of the Oliveira and Martinho labs for fruitful discussions. We thank the dedicated facilities at Instituto Gulbenkian de Ciência (IGC): Fly Facility, the Advanced Imaging Facility (AIF) and the Technical Support Service. Especial thanks to Stefan Heidmann (Univ. Bayreuth), Michael Levine (Princeton Univ.) and the Bloomington *Drosophila* Stock Center (BDSC) for fly stocks. This work was supported by the following bodies: European Research Council (ERC) under the European Union's Horizon 2020 research and innovation programme (grant agreement No 101002391) to R.A.O., Fundação para Ciência e a Tecnologia (FCT) supporting C.C. (PD/BD/128428/2017), R.A.O. (CEECIND/01092/2017 and 2022.01782.PTDC), R.D.S (DL57/2016/CP1361/CT0019), R.G.M (PTDC/BIA-BID/1606/2020); Fundação Calouste Gulbenkian (FCG) and LISBOA-01-0145-FEDER-007654 supporting IGC's core operation; LISBOA-01-7460145-FEDER-022170 (Congento) supporting the IGC Fly Facility; PPBI-POCI-01-0145-FEDER-022122 supporting the IGC Advanced Imaging Facility, all co-financed by FCT (Portugal) and Lisboa Regional Operational Program (Lisboa2020) under the PORTUGAL2020 Partnership Agreement (European Regional Development Fund). The funders had no role in study design, data collection and interpretation, and are not responsible for any use that may be made of the information in this manuscript.

Author contributions
Catarina Carmo: Conceptualization; formal analysis; investigation; writing – review and editing. **João Coelho:** Conceptualization; formal analysis; investigation; methodology; writing – review and editing. **Rui D Silva:** Conceptualization; formal analysis; investigation; methodology; writing – review and editing. **Alexandra Tavares:** Resources; formal analysis; investigation; methodology; writing – review and editing. **Ana Boavida:** Formal analysis; investigation. **Paola Gaetani:** Formal analysis; investigation. **Leonardo G Guilgur:** Investigation; methodology. **Rui Gonçalo Martinho:** Conceptualization; supervision; funding acquisition; writing – review and editing. **Raquel A Oliveira:** Conceptualization; formal analysis; supervision; funding acquisition; writing – original draft.

Disclosure and competing interests statement
The authors declare that they have no conflict of interest.

References

Akoulitchev S, Reinberg D (1998) The molecular mechanism of mitotic inhibition of TFIIH is mediated by phosphorylation of CDK7. *Genes Dev* 12: 3541–3550

Ball CB, Parida M, Santana JF, Spector BM, Suarez GA, Price DH (2022) Nuclear export restricts Gdown1 to a mitotic function. *Nucleic Acids Res* 50: 1908–1926

Baumann C, Korner R, Hofmann K, Nigg EA (2007) PICH, a centromere-associated SNF2 family ATPase, is regulated by Plk1 and required for the spindle checkpoint. *Cell* 128: 101–114

Baxter J, Sen N, Martinez VL, De Carandini ME, Schvartzman JB, Diffley JF, Aragon L (2011) Positive supercoiling of mitotic DNA drives decatenation by topoisomerase II in eukaryotes. *Science* 331: 1328–1332

Bellier S, Chastant S, Adenot P, Vincent M, Renard JP, Bensaude O (1997) Nuclear translocation and carboxyl-terminal domain phosphorylation of RNA polymerase II delineate the two phases of zygotic gene activation in mammalian embryos. *EMBO J* 16: 6250–6262

Berrocal A, Lammers NC, Garcia HG, Eisen MB (2020) Kinetic sculpting of the seven stripes of the drosophila even-skipped gene. *Elife* 9: e61635

Brandao HB, Paul P, van den Berg AA, Rudner DZ, Wang X, Mirny LA (2019) RNA polymerases as moving barriers to condensin loop extrusion. *Proc Natl Acad Sci USA* 116: 20489–20499

Carmo C, Araujo M, Oliveira RA (2019) Microinjection techniques in Fly embryos to study the function and dynamics of SMC complexes. *Methods Mol Biol* 2004: 251–268

Cho CY, Kemp JP Jr, Duronio RJ, O'Farrell PH (2022) Coordinating transcription and replication to mitigate their conflicts in early drosophila embryos. *Cell Rep* 41: 111507

Christensen MO, Larsen MK, Barthelmes HU, Hock R, Andersen CL, Kjeldsen E, Knudsen BR, Westergaard O, Boege F, Mielke C (2002) Dynamics of human DNA topoisomerases IIalpha and IIbeta in living cells. *J Cell Biol* 157: 31–44

Davidson IF, Bauer B, Goetz D, Tang W, Wutz G, Peters JM (2019) DNA loop extrusion by human cohesin. *Science* 366: 1338–1345

Doren MV, Williamson AL, Lehmann R (1998) Regulation of zygotic gene expression in Drosophila primordial germ cells. *Current Biology* 8(4): 243–246

Durr H, Flaus A, Owen-Hughes T, Hopfner KP (2006) Snf2 family ATPases and DExx box helicases: differences and unifying concepts from high-resolution crystal structures. *Nucleic Acids Res* 34: 4160–4167

Eichinger CS, Kurze A, Oliveira RA, Nasmyth K (2013) Disengaging the Smc3/kleisin interface releases cohesin from *Drosophila* chromosomes during interphase and mitosis. *EMBO J* 32: 656–665

Farcas AM, Uluocak P, Helmhart W, Nasmyth K (2011) Cohesin's concatenation of sister DNAs maintains their intertwining. *Mol Cell* 44: 97–107

Fukaya T, Lim B, Levine M (2017) Rapid rates of pol II elongation in the *Drosophila* embryo. *Curr Biol* 27: 1387–1391

Gandhi R, Gillespie PJ, Hirano T (2006) Human Wapl is a cohesin-binding protein that promotes sister-chromatid resolution in mitotic prophase. *Curr Biol* 16: 2406–2417

Ganji M, Shaltiel IA, Bisht S, Kim E, Kalichava A, Haering CH, Dekker C (2018) Real-time imaging of DNA loop extrusion by condensin. *Science* 360: 102–105

Garcia HG, Tikhonov M, Lin A, Gregor T (2013) Quantitative imaging of transcription in living *Drosophila* embryos links polymerase activity to patterning. *Curr Biol* 23: 2140–2145

Gebara MM, Sayre MH, Corden JL (1997) Phosphorylation of the carboxy-terminal repeat domain in RNA polymerase II by cyclin-dependent kinases is sufficient to inhibit transcription. *J Cell Biochem* 64: 390–402

Gimenez-Abian JF, Sumara I, Hirota T, Hauf S, Gerlich D, de la Torre C, Ellenberg J, Peters JM (2004) Regulation of sister chromatid cohesion between chromosome arms. *Curr Biol* 14: 1187–1193

Girdham CH, Glover DM (1991) Chromosome tangling and breakage at anaphase result from mutations in lodestar, a *Drosophila* gene encoding a putative nucleoside triphosphate-binding protein. *Genes Dev* 5: 1786–1799

Gompel N, Schröder EA (2015) *Drosophila* germline transformation. (http://gompel.org/wp-content/uploads/2021/04/Drosophila-transformation-with-chorion.pdf)

Gottesfeld JM, Forbes DJ (1997) Mitotic repression of the transcriptional machinery. *Trends Biochem Sci* 22: 197–202

Hou F, Chu CW, Kong X, Yokomori K, Zou H (2007) The acetyltransferase activity of San stabilizes the mitotic cohesin at the centromeres in a shugoshin-independent manner. *J Cell Biol* 177: 587–597

Jiang Y, Liu M, Spencer CA, Price DH (2004) Involvement of transcription termination factor 2 in mitotic repression of transcription elongation. *Mol Cell* 14: 375–385

Kim Y, Shi Z, Zhang H, Finkelstein IJ, Yu H (2019) Human cohesin compacts DNA by loop extrusion. *Science* 366: 1345–1349

Kleinschnitz K, Viessmann N, Jordan M, Heidmann SK (2020) Condensin I is required for faithful meiosis in *Drosophila* males. *Chromosoma* 129: 141–160

Kondo S, Ueda R (2013) Highly improved gene targeting by germline-specific Cas9 expression in *Drosophila*. *Genetics* 195: 715–721

Kueng S, Hegemann B, Peters BH, Lipp JJ, Schleiffer A, Mechtler K, Peters JM (2006) Wapl controls the dynamic association of cohesin with chromatin. *Cell* 127: 955–967

Liang HL, Nien CY, Liu HY, Metzstein MM, Kirov N, Rushlow C (2008) The zinc-finger protein Zelda is a key activator of the early zygotic genome in *Drosophila*. *Nature* 456: 400–403

Liang K, Woodfin AR, Slaughter BD, Unruh JR, Box AC, Rickels RA, Gao X, Haug JS, Jaspersen SL, Shilatifard A (2015) Mitotic transcriptional activation: clearance of actively engaged pol II via transcriptional elongation control in mitosis. *Mol Cell* 60: 435–445

Liu M, Xie Z, Price DH (1998) A human RNA polymerase II transcription termination factor is a SWI2/SNF2 family member. *J Biol Chem* 273: 25541–25544

Long JJ, Leresche A, Kriwacki RW, Gottesfeld JM (1998) Repression of TFIIH transcriptional activity and TFIIH-associated cdk7 kinase activity at mitosis. *Mol Cell Biol* 18: 1467–1476

Losada A, Hirano M, Hirano T (1998) Identification of Xenopus SMC protein complexes required for sister chromatid cohesion. *Genes Dev* 12: 1986–1997

Nakazawa N, Arakawa O, Yanagida M (2019) Condensin locates at transcriptional termination sites in mitosis, possibly releasing mitotic transcripts. *Open Biol* 9: 190125

Ng M, Diaz-Benjumea FJ, Vincent JP, Wu J, Cohen SM (1996) Specification of the wing by localized expression of wingless protein. *Nature* 381: 316–318

Oliveira RA, Heidmann S, Sunkel CE (2007) Condensin I binds chromatin early in prophase and displays a highly dynamic association with *Drosophila* mitotic chromosomes. *Chromosoma* 116: 259–274

Oliveira RA, Hamilton RS, Pauli A, Davis I, Nasmyth K (2010) Cohesin cleavage and Cdk inhibition trigger formation of daughter nuclei. *Nat Cell Biol* 12: 185–192

Oliveira RA, Kotadia S, Tavares A, Mirkovic M, Bowlin K, Eichinger CS, Nasmyth K, Sullivan W (2014) Centromere-independent accumulation of cohesin at ectopic heterochromatin sites induces chromosome stretching during anaphase. *PLoS Biol* 12: e1001962

Perea-Resa C, Bury L, Cheeseman IM, Blower MD (2020) Cohesin removal reprograms gene expression upon mitotic entry. *Mol Cell* 78: 127–140.e7

Piskadlo E, Oliveira RA (2016) Novel insights into mitotic chromosome condensation. *F1000Res* 5: https://doi.org/10.12688/f1000research.8727.1

Piskadlo E, Oliveira RA (2017) A topology-centric view on mitotic chromosome architecture. *Int J Mol Sci* 18: 2751

Piskadlo E, Tavares A, Oliveira RA (2017) Metaphase chromosome structure is dynamically maintained by condensin I-directed DNA (de)catenation. *Elife* 6: e26120

Pitchai GP, Kaulich M, Bizard AH, Mesa P, Yao Q, Sarlos K, Streicher WW, Nigg EA, Montoya G, Hickson ID (2017) A novel TPR-BEN domain interaction mediates PICH-BEND3 association. *Nucleic Acids Res* 45: 11413–11424

Pommier Y, Sun Y, Huang SN, Nitiss JL (2016) Roles of eukaryotic topoisomerases in transcription, replication and genomic stability. *Nat Rev Mol Cell Biol* 17: 703–721

Price DH, Sluder AE, Greenleaf AL (1987) Fractionation of transcription factors for RNA polymerase II from drosophila kc cell nuclear extracts. *J Biol Chem* 262: 3244–3255

Pritchard DK, Schubiger G (1996) Activation of transcription in drosophila embryos is a gradual process mediated by the nucleocytoplasmic ratio. *Genes Dev* 10: 1131–1142

Ribeiro AL, Silva RD, Foyn H, Tiago MN, Rathore OS, Arnesen T, Martinho RG (2016) Naa50/san-dependent N-terminal acetylation of Scc1 is potentially important for sister chromatid cohesion. *Sci Rep* 6: 39118

Rong Z, Ouyang Z, Magin RS, Marmorstein R, Yu H (2016) Opposing functions of the N-terminal acetyltransferases Naa50 and NatA in sister-chromatid cohesion. *J Biol Chem* 291: 19079–19091

Rothe M, Pehl M, Taubert H, Jackle H (1992) Loss of gene function through rapid mitotic cycles in the *Drosophila* embryo. *Nature* 359: 156–159

Ryoo HD, Gorenc T, Steller H (2004) Apoptotic cells can induce compensatory cell proliferation through the JNK and the wingless signaling pathways. *Dev Cell* 7: 491–501

Schuh M, Lehner CF, Heidmann S (2007) Incorporation of drosophila CID/CENP-A and CENP-C into centromeres during early embryonic anaphase. *Curr Biol* 17: 237–243

Segil N, Guermah M, Hoffmann A, Roeder RG, Heintz N (1996) Mitotic regulation of TFIID: inhibition of activator-dependent transcription and changes in subcellular localization. *Genes Dev* 10: 2389–2400

Sen N, Leonard J, Torres R, Garcia-Luis J, Palou-Marin G, Aragon L (2016) Physical proximity of sister chromatids promotes Top2-dependent intertwining. *Mol Cell* 64: 134–147

Sharp JA, Perea-Resa C, Wang W, Blower MD (2020) Cell division requires RNA eviction from condensing chromosomes. *J Cell Biol* 219: e201910148

Shermoen AW, O'Farrell PH (1991) Progression of the cell cycle through mitosis leads to abortion of nascent transcripts. *Cell* 67: 303–310

Silva RD, Mirkovic M, Guilgur LG, Rathore OS, Martinho RG, Oliveira RA (2018) Absence of the spindle assembly checkpoint restores mitotic fidelity upon loss of sister chromatid cohesion. *Curr Biol* 28: 2837–2844.e3

Spence JM, Phua HH, Mills W, Carpenter AJ, Porter AC, Farr CJ (2007) Depletion of topoisomerase IIalpha leads to shortening of the metaphase interkinetochore distance and abnormal persistence of PICH-coated anaphase threads. *J Cell Sci* 120: 3952–3964

Staudt N, Fellert S, Chung HR, Jackle H, Vorbruggen G (2006) Mutations of the drosophila zinc finger-encoding gene vielfaltig impair mitotic cell divisions and cause improper chromosome segregation. *Mol Biol Cell* 17: 2356–2365

Sumara I, Vorlaufer E, Gieffers C, Peters BH, Peters JM (2000) Characterization of vertebrate cohesin complexes and their regulation in prophase. *J Cell Biol* 151: 749–762

Szalontai T, Gaspar I, Belecz I, Kerekes I, Erdelyi M, Boros I, Szabad J (2009) HorkaD, a chromosome instability-causing mutation in *Drosophila*, is a dominant-negative allele of lodestar. *Genetics* 181: 367–377

Tadros W, Lipshitz HD (2009) The maternal-to-zygotic transition: a play in two acts. *Development* 136: 3033–3042

Tavormina PA, Come MG, Hudson JR, Mo YY, Beck WT, Gorbsky GJ (2002) Rapid exchange of mammalian topoisomerase II alpha at kinetochores and chromosome arms in mitosis. *J Cell Biol* 158: 23–29

Wiegard A, Kuzin V, Cameron DP, Grosser J, Ceribelli M, Mehmood R, Ballarino R, Valant F, Grochowski R, Karabogdan I *et al* (2021) Topoisomerase 1 activity during mitotic transcription favors the transition from mitosis to G1. *Mol Cell* 81: 5007–5024.e9

Williams BC, Garrett-Engele CM, Li Z, Williams EV, Rosenman ED, Goldberg ML (2003) Two putative acetyltransferases, san and deco, are required for establishing sister chromatid cohesion in *Drosophila*. *Curr Biol* 13: 2025–2036

Wu J, Cohen SM (2002) Repression of Teashirt marks the initiation of wing development. *Development* 129: 2411–2418

Xie Z, Price DH (1996) Purification of an RNA polymerase II transcript release factor from *Drosophila*. *J Biol Chem* 271: 11043–11046

Xie Z, Price D (1997) Drosophila factor 2, an RNA polymerase II transcript release factor, has DNA-dependent ATPase activity. *J Biol Chem* 272: 31902–31907

Xie Z, Price DH (1998) Unusual nucleic acid binding properties of factor 2, an RNA polymerase II transcript release factor. *J Biol Chem* 273: 3771–3777

Xing H, Vanderford NL, Sarge KD (2008) The TBP-PP2A mitotic complex bookmarks genes by preventing condensin action. *Nat Cell Biol* 10: 1318–1323